Clays and Clay Minerals, Vol. 64, No. 2, 145–166, 2016.

MINERALOGY, GEOCHEMISTRY, AND GENESIS OF SEPIOLITE AND PALYGORSKITE IN NEOGENE LACUSTRINE SEDIMENTS, ESKİŞEHİR PROVINCE, WEST CENTRAL ANATOLIA, TURKEY

Selahattin Kadir[1], Hülya Erkoyun[1], Muhsin Eren[2], Jennifer Huggett[3], and Nergis Önalgil[1]

[1] Eskişehir Osmangazi University, Department of Geological Engineering, TR-26480 Eskişehir, Turkey
[2] Mersin University, Department of Geological Engineering, TR-33343, Mersin, Turkey
[3] Department of Earth Sciences, Natural History Museum, Cromwell Road, London SW7 5BD, UK

Abstract—Sepiolite and palygorskite are common as layers and nodules in the Neogene lacustrine sediments of the Eskişehir area. This study aims to determine their mineralogical and geochemical characteristics, plus the distribution of these economically important sepiolite and palygorskite deposits within the lacustrine environment. Using these data the research goes on to discuss the environmental conditions for their formation. Sepiolite and palygorskite layers are associated with dolomite, marlstone, and argillaceous limestone. The sepiolite nodules (meerschaum), which are former magnesite gravels, are observed in the Upper Miocene reddish-brown fluvial deposits derived from the ophiolite and its fracture-infills at the northern margin of the basin. Sepiolite and palygorskite are only sparsely associated with dolomite and accessory magnesite, quartz, feldspar, and amphibole. Sepiolite and palygorskite fibers formed as oriented platy fan, interwoven, and knitted aggregates in the absence of dolomite indicated precipitation from supersaturated solution. Sepiolite and palygorskite fibers edging dolomite crystals post-date dolomite and formed through precipitation in a vadose environment under semi-arid to arid climatic conditions. High values of Mg+Fe+Ni and enrichment of light rare earth elements (*LREE*) relative to middle rare earth elements (*MREE*) and heavy rare earth elements (*HREE*), Sr content, depletion of Rb+Ba and K, and negligible negative Eu anomalies all reflect the derivation from the Paleozoic metamorphic and Upper Cretaceous ophiolitic rocks. Locally, Upper Miocene to Lower Pliocene volcanic, volcanoclastic, and fluvio-lacustrine sedimentary rocks supplied the required Si, Mg, Al, and Fe for precipitation of Al-sepiolite and Mg-palygorskite with average structural formulae of $Si_{11.91}Al_{0.09}O_{30}Mg_{6.60}Al_{0.78}Fe_{0.13}(OH)_4Na_{0.12}K_{0.06}(OH_2)_4{\cdot}nH_2O$ and $Si_{7.74}Al_{0.26}O_{20}Mg_{2.52}Al_{1.13}Fe_{0.38}(OH)_2(OH_2)_4Na_{0.32}K_{0.14}Ca_{0.12}{\cdot}nH_2O$, respectively. In contrast to the layered sepiolites, the absence of Al and high Ni content in sepiolite nodules suggest formation through replacement of magnesite gravels at shallow burial in an alkaline environment. The calculated meerschaum sepiolite chemical formula is: $Si_{12.02}O_{30}Mg_{7.87}Fe_{0.01}(OH)_4Na_{0.13}K_{0.03}(OH_2)_4{\cdot}nH_2O$.

Key Words—Argillaceous Carbonate, Dolomite, Eskişehir, Meerschaum Sepiolite, Neogene, Palygorskite, Sepiolite, Turkey.

INTRODUCTION

Sepiolite deposits in the Eskişehir province (west central Anatolia) have been known since the 18th century (İrkeç and Gençoğlu, 1993; Ece and Çoban, 1994; Ece, 1998; Kadir *et al*., 2002, 2010; Karakaya *et al.*, 2004, 2011; Yeniyol, 2012, 2014), while sepiolite nodules (meerschaum) have been exploited in Anatolia since ancient times (Bilgen, 2006). Meerschaum sepiolite has physical properties that have made it a valued material for the carving of highly decorative and lustrous smoking pipes and ornaments.

Sepiolite nodules and layers associated with dolomite are overlain by Lower Pliocene gypsum-bearing dolomite in the lacustrine sediments (Akıncı, 1967). Sepiolite and palygorskite layers are brown, beige, and white in color. The darkness of the layers depends on the relative abundance of sepiolite ± palygorskite, organic material, and dolomite content (Fukushima and Shimosaka, 1987; İrkeç, 1987–1988). Sepiolite and palygorskite precipitated from lake (Singer, 1984, 1989; Rodas *et al.*, 1994; Galán and Pozo, 2011) and/or interstitial waters between magnesian silicate precursors and dolomitic sediments under saline, alkaline (pH 8.0–9.5), and low pCO_2 conditions during early diagenesis (Jones and Galán, 1988; Akbulut and Kadir, 2003).

Palygorskite is commonly formed from aluminous-magnesian smectitic precursors or through precipitation from solution in lacustrine-palustrine, ephemeral-playa enviroments, paleosols, and calcretes (Jones and Galán, 1988; Eren *et al.*, 2004, 2008; Kadir and Eren, 2008; Kaplan *et al.*, 2014; among others) under shallow evaporitic conditions associated with carbonate, sulfate, and rarely phosphate minerals (Singer and Norrish, 1974; Post, 1978; Singer, 1979; Galán and Ferrero, 1982; Singer, 1984; Shadfan *et al.*, 1985; Yeniyol, 1986; Jones and Galán, 1988; İrkeç and Ünlü, 1993; Suárez *et*

* E-mail address of corresponding author:
skadir_esogu@yahoo.com
DOI: 10.1346/CCMN.2016.0640206

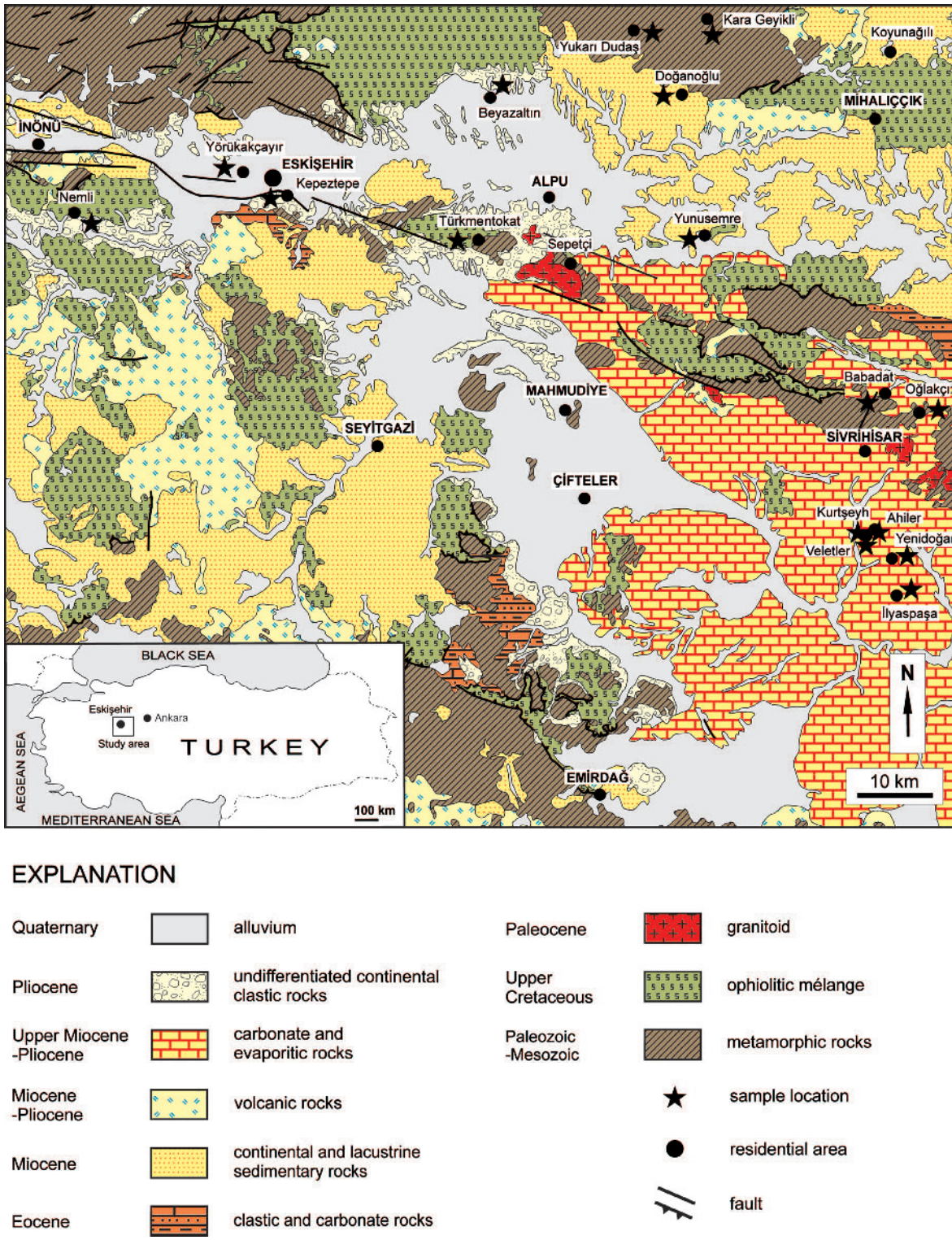

Figure 1. Geological map of the Eskişehir region with sample locations (after Konak, 2002; Turhan, 2002; reproduced with the kind permission of the General Directorate of Mineral Research and Exploration, Turkey).

https://doi.org/10.1346/CCMN.2016.0640206 Published online by Cambridge University Press

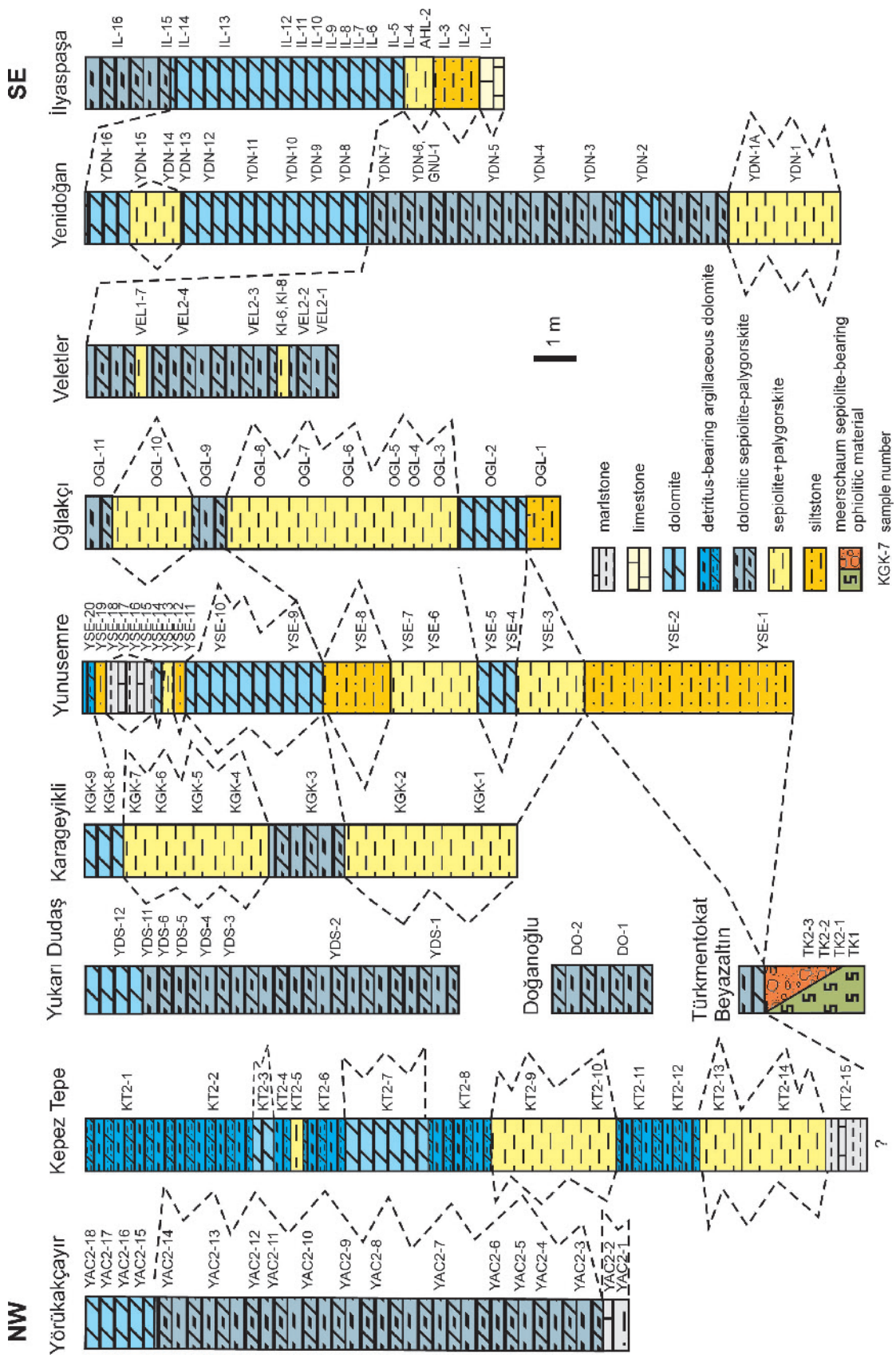

Figure 2. Measured stratigraphic sections showing vertical and lateral distribution of lithologies in the Eskişehir area.

https://doi.org/10.1346/CCMN.2016.0640206 Published online by Cambridge University Press

al., 1994; Webster and Jones, 1994; Pozo and Casas, 1999).

To date, the Eskişehir region has been studied mainly for the geology, mineralogy (powder X-ray diffraction, scanning electron microscopy, differential thermal and thermogravimetry analyses, infrared spectra), and geochemistry (major oxide) of its sepiolite and palygorskite deposits. Samples were obtained from the northwest (Akçayır-Yörükakçayır-Kepeztepe) (Akıncı, 1967; Sarıiz, 2000; Yeniyol, 2012), the northeast (Margı, Koyunağılı), and the southeast (Türkmentokat-Sarısu, Kurtşeyh, Ahiler, İlyaspaşa, Oğlakçı, Yenidoğan) (Karakaş, 1992; Yeniyol, 1992, 1993; ITIT, 1993; Ece and Çoban, 1994; Gençoğlu, 1996; Saraç *et al*., 1996; Yeniyol, 2014) of the Eskişehir Neogene lacustrine sediments. Prior to the present study, no analysis had been reported regarding the origin or the lateral variability, from basin center to margin, of the mineralogy and geochemistry of the sepiolite and palygorskite in these lacustrine sediments, or regarding the meerschaum sepiolite within the fluvial channel sediments. The new data in the present study will be used to discuss the environmental conditions for the formation of these sepiolite, meerschaum sepiolite, and palygorskite deposits, which have economic potential. Furthermore, these new data and interpretations will guide future exploration of similar sepiolite and palygorskite deposits and related Neogene lacustrine sediments worldwide.

GEOLOGICAL SETTING

The basement rocks in the Eskişehir area comprise Paleozoic-Mesozoic metamorphics (sericite and glaucophane schists and marbles), Upper Cretaceous ophiolitic rocks (serpentinized harzburgites, pyroxenites, gabbros, and serpentinites), and Upper Cretaceous to Paleocene granitoid rocks (Figures 1 and 2; Kulaksız, 1981; Yılmaz, 1981; Gözler *et al*., 1996). The basement rocks are overlain unconformably by Upper Miocene to Lower Pliocene volcanic, volcanoclastic, and fluviolacustrine sedimentary rocks. The Upper Miocene İlyaspaşa Formation in the study area is represented by shale, marlstone, carbonate, tuff, and gypsum beds. The Lower Pliocene rocks of the Sakarya Formation consist of reddish-brown sandy clays, gypsum-bearing green claystone, alternation of dolomitic marlstone and sepiolite-palygorskite as lenses and horizontal layers and dolomite, and at the top by fossiliferous limestone (Yeniyol, 2007, 2012; ITIT, 1993). Organic material, root imprints, and lignite associated with brown and black claystone lenses increase basinward, indicating an anaerobic, swampy, shallow lacustrine depositional environment. Claystone, argillaceous dolomite, dolomite, limestone, and crystalline gypsum alternate, and increase in thickness and abundance basinward, whereas limestone, sandy limestone, gypsum lenses, thinner dolomite layers, and sandy and silty detrital material increase in abundance toward the paleo-lake margin (Figure 2). This lateral distribution is progressive and gradual. Sepiolite color is controlled by carbonate and organic material, and ranges from black-brown to beige or white.

In some places, white to beige colored sepiolite nodules are observed within the Pliocene reddish-brown detrital sediments, which are mainly breccia, unconformably overlying the ophiolitic rocks at the northern margin of the basin. Ophiolitic rocks contain vein-, lens-, massif-, and breccia-type magnesite (Öncel and Denizci, 1982; Yeniyol and Öztunalı, 1985; Yeniyol, 1993; Ece and Çoban, 1994; Özbaş, 2008).

The study area is part of the central Anatolian Neogene basin, which has been affected by N−S- and related E−W- or WNW−ESE-trending tensional and compressional tectonics (Eskişehir Fault Zone, Figure 1) between the strike-slip North Anatolian Fault Zone and the western Anatolian extensional region, resulting from the collision between the Eurasian and Arabian plates during the Late Miocene and Early Pliocene (Şengör and Yılmaz, 1981; Şengör *et al*., 1985). Consequently, synsedimentary depressional zones became sites of tectonically controlled deposition, including gypsum-bearing green claystone and dolomite, with sepiolite in shallow environments of increased evaporation.

DESCRIPTION OF SEPIOLITE AND PALYGORSKITE DEPOSITS AND OCCURRENCES

Nemli (NM), Kepeztepe (KT), and Yörükakçayır (YAC) regions

The white and beige colored meerschaum sepiolite nodules with diameters of 0.5−15 cm are common in the Upper Miocene reddish-brown fluvial sediments consisting mainly of ophiolitic materials in the Nemli region (Figures 1 [base map reproduced with the kind permission of the General Directorate of Mineral Research and Exploration, Turkey], 2). These sediments are overlain by claystone, dolomitic sepiolite, sepiolitic dolomite, and/or dolomite in Kepeztepe. Beige-red friable carbonaceous claystone occurs at the bottom of the sequence.

Figure 3 (*facing page*). Field photographs of sepiolite and palygorskite in the Eskişehir region: (a) meerschaum nodule in ophiolitic materials in the Türkmentokat pit; (b) close-up view of a; (c) brown sepiolite lenses in beige dolomitic sepiolite and palygorskite layers in the Karageyikli pit; (d,e) organic matter-bearing brown sepiolite in white sepiolitic dolomite in the Yunusemre pit; (f) brown sepiolite lens between beige and white dolomitic sepiolite layers in the Oğlakçı pit; (g) occurrence of organic-bearing brown sepiolite between white sepiolitic dolomitic layers in the Veletler pit; (h) close-up view of brown sepiolite in the Yenidoğan pit.

https://doi.org/10.1346/CCMN.2016.0640206 Published online by Cambridge University Press

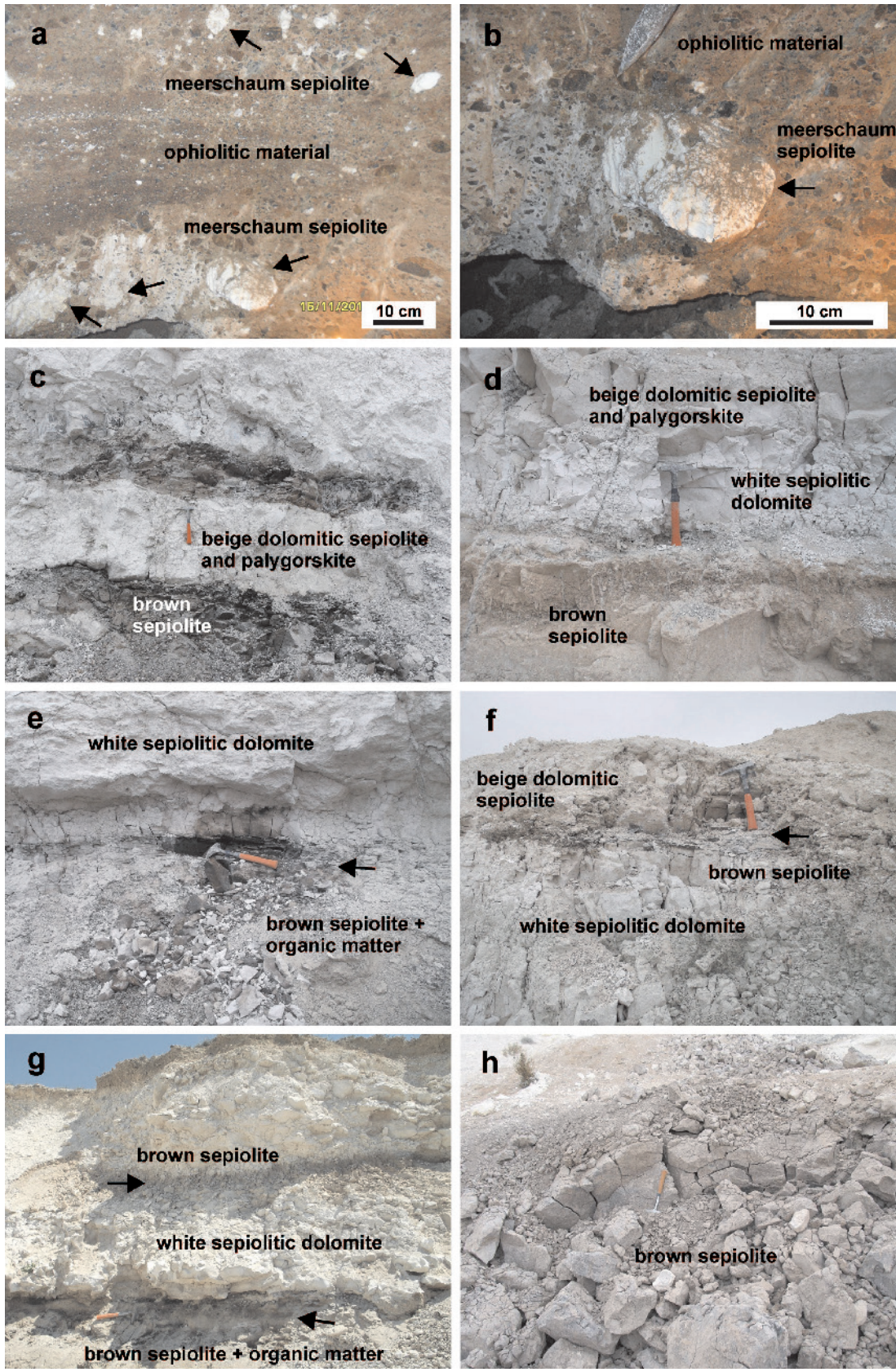

https://doi.org/10.1346/CCMN.2016.0640206 Published online by Cambridge University Press

Table 1. Semi-quantitative mineralogical compositions of the samples in the Eskişehir area.

	sep	plg	sme	chl/kln	ilt/mca	cal	dol	mgs	qz	fsp	amp
Yörükakçayır											
YAC1-2		+	++++						acc		
YAC1-4		+	++++						acc		
YAC1-9	acc	+	+++				+		acc		
YAC1-13	+						++++				
YAC2-3		+	++				++		acc		
YAC2-8		++	+++				+		acc		
YAC2-12			+++				++				
YAC2-13	++	+					++				
YAC2-15		++	+++								
Kepeztepe											
KT1-1		++					++		+		
KT2-9	+		+				+++		acc		
KT2-13		++++			acc		+		+	acc	
KT2-15			++				+++		acc		
Nemli											
NM-1	+						++++		acc		
NM-2	+++						++				
NM-3	+	+					+	+			
Yukarı Dudaş											
YDS-1	++						+	++			
YDS-2	+++						++	+			
YDS-3			+++				+	+			
YDS-4	++		+				++	+	acc		
YDS-5		++		+		+	++			acc	acc
YDS-6	+	+				+	++		acc	acc	acc
YDS-11	+++						++				
Karageyikli											
KGK-1		+++							+	+	
KGK-2		++++							+	acc	
KGK-3	+	++							+	+	
KGK-4		+++							+	+	acc
KGK-5	++	++					++		+	+	
KGK-6	+	+++				+			+	acc	
KGK-7	++	+++			acc	+			+	+	
KGK-8		+					++++		acc		
KGK-9	+						++++				
Doğanoğlu											
DO-11	++						+++				
DO-12	++						+++				
Türkmentokat											
TK1	++++						+				
TK2-1	+++++										
TK2-2	+++++					acc					
TK2-3	+++						++				
Yunusemre											
YSE-1		++++							+		
YSE-2	+						++++				
YSE-3	++	+++					+		acc	+	
YSE-8	++						+++		+		
YSE-11			+++				++				
YSE-17			+++				++				
Oğlakçı											
OGL-1		++		++			+		+	acc	
OGL-2	+	acc		acc	acc		+++			acc	
OGL-4	+++++										
OGL-7	+++						++				
OGL-10	++						+++				

https://doi.org/10.1346/CCMN.2016.0640206 Published online by Cambridge University Press

Table 1 (*contd.*)

	sep	plg	sme	chl/kln	ilt/mca	cal	dol	mgs	qz	fsp	amp
Veletler											
VEL1-7	+++++						acc			acc	acc
VEL2-2	++						+++			acc	
KI-6	+++++						acc				
KI-8	++++									+	
Yenidoğan											
YDN-1	++++								acc	acc	
YDN-1A	++++								+	acc	
YDN-3	+++						++				
YDN-4	+++		+				+				
YDN-8	+++		+				+				
YDN-14	+		+++				+				
İlyaspaşa											
AHL-2			++++							acc	
IL-15	++++					acc	+				

+: relative abundance of mineral. sep: sepiolite, plg: palygorskite, sme: smectite, chl/kln: chlorite/kaolinite, ilt/mca: illite/mica, cal: calcite, dol: dolomite, mgs: magnesite, qz: quartz, fsp: feldspar, amp: amphibole, acc: accessory (mineral-name abbreviations after Whitney and Evans, 2010).

This unit is overlain by 2 m-thick, dark-beige plastic claystone. The sepiolite and/or palygorskite units exhibit brown color, moderate hardness, and conchoidal fracture, and are 1–1.5 m thick. The dolomitic sepiolite is 2 m thick, beige in color, moderately hard, and plastic in character, and exhibits wide lateral extent. The proportion of dolomite increases up section.

Türkmentokat-Beyazaltın (TK) region

In 2–7 m-deep wells, the white, soft, and pure meerschaum sepiolite nodules with a diameter commonly of 4–10 and up to 20 cm are observed in the bright brown-beige fluvial sediments derived from ophiolitic materials (Figures 3a,b). These materials also enclose subangular magnesite pebbles derived from vein- and stockwork-type magnesite deposits within ophiolite units.

Yukarı Dudaş (YDS), Karageyikli (KGK), and Doğanoğlu (DO) regions

The grayish-beige, compact dolomitic sepiolite occurs at the bottom of the sequence (Figures 1, 2, 3c). This unit is overlain by 1.5 to 5 m-thick, compact, grayish white sepiolitic dolomite containing 40 cm-thick subvertical greenish-gray, friable smectitic claystone exhibiting desiccation cracks up section. The sepiolitic units in the pits around the Yukarı Dudaş village are mined for use as pet-litter by the Sakarya Minerals Company.

The brown sepiolite lenses showing conchoidal fracture occur at the bottom of an inactive open pit near the Karageyikli village (Figure 3c). This unit is overlain by 1.5 m thick greenish-brown sepiolite, also with a conchoidal fracture, and bearing root imprints. At the top of the succesion is a white-beige, sepiolitic and hard dolomite.

The white-beige sepiolitic dolomite at the bottom of the sequence in the Doğanoğlu village is friable with abundant desiccation cracks. This unit is 1.5 m thick, is laterally extensive, and is overlain by hard beige 2 m-thick sepiolitic dolomite with solution cavities.

Yunusemre (YSE) and Oğlakçı (OGL) regions

A brown-beige colored and compact sepiolite unit occurs at the base of the open pit in the Yunusemre (Yalınlı) region (Figures 1, 2, and 3d,e). The sepiolite-palygorskite-bearing unit includes dark greyish-black laminae of organic matter (Figure 3e,g). This unit gradually passes to loose, white-beige, 0.5–2 m-thick dolomitic sepiolite and sepiolitic dolomite. The proportion of carbonate increases up section. The 0.2–2 m-thick dolomite has a white-beige color, is partially argillic, and locally hard, with solution cavities occurring in the uppermost beds.

A green, plastic claystone occurs at the base of the sequence in the Oğlakçı sepiolite pit. This unit is overlain by 1.5–2 m-thick white-beige, moderately hard sepiolitic dolomite with abundant desiccation cracks and 5–15 cm-thick, lenticular brown sepiolite (Figure 3f). The beige and brown sepiolite alternation increases in the upper levels. Hard sepiolitic dolomite occurs at the top of the succession.

Veletler (VEL and KI) and İlyaspaşa (IL and AHL) regions

A white dolomitic sepiolite unit with conchoidal fracture occurs in the Veletler sepiolite pit (Figure 1). This unit alternates with hard, white-beige dolomitic

https://doi.org/10.1346/CCMN.2016.0640206 Published online by Cambridge University Press

units towards the top of the interval (Figures 1, 2, 3g). Locally, the 0.5–1 m-thick beige sepiolite alternates with a 1–2 m-thick brown sepiolite exhibiting conchoidal fracture.

A hard, beige limestone with solution cavities is present at the base of the exposed interval in the İlyaspaşa region. This unit is overlain by a 1 m-thick, brown sepiolite, a 5 m-thick, hard beige dolomite, and a

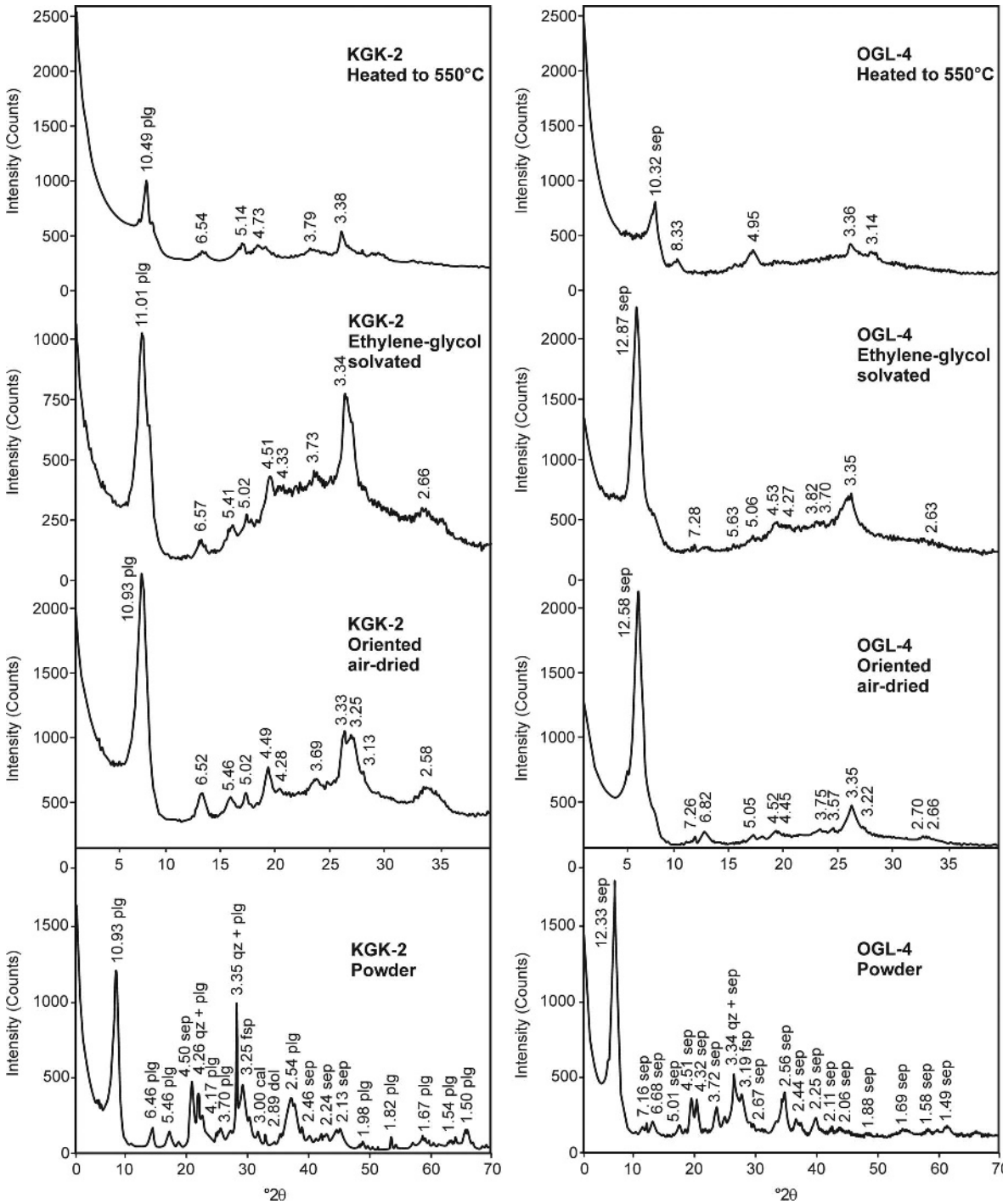

Figure 4 (*this and facing page*). X-ray diffraction patterns (CuKα) of the samples in the Eskişehir area. sep: sepiolite, plg: palygorskite, cal: calcite, dol: dolomite, qz: quartz, fsp: feldspar, amp: amphibole (mineral-name abbreviations after Whitney and Evans, 2010). Interplanar spacings are in Å units.

https://doi.org/10.1346/CCMN.2016.0640206 Published online by Cambridge University Press

2 m dolomitic sepiolite, and contains 0.1–15 cm-thick gypsum crystals up section.

Yenidoğan (YDN) region

A brown colored sepiolite unit occurs at the base of the pit in the Yenidoğan region (Figures 1, 2, and 3h). The 0.2–1 m-thick brown sepiolite alternates with white-beige, loose, 0.3–1.5 m-thick sepiolite. The hard white-beige dolomitic units at the top of the interval are laterally extensive.

MATERIALS AND METHODS

Representative stratigraphic sections were studied to investigate vertical and lateral variations within the sepiolite layers and nodules (meerschaum), and palygorskite deposits in the Eskişehir Neogene basin. The mineralogical and petrographic characteristics of the samples were determined by powder X-ray diffraction (XRD) (Rigaku D/Max–2200 Ultia PC, Japan), scanning electron microscopy with energy dispersive X-ray spectroscopy (SEM-EDX) (JEOL JSM 5600LV, Japan), and transmission electron microscopy (TEM) (JEOL JEM-21007, Japan). The clay mineralogy was determined after separation of the clay fraction (<2 μm) by sedimentation, followed by centrifugation of the suspension after an overnight dispersion in distilled water. The clay particles were dispersed by ultrasonic vibration for ~15 min. Three oriented specimens of the <2 μm fraction of each sample were prepared by air drying, ethylene-glycol solvation at 60ºC for 2 h, and thermal treatment at 550ºC for 2 h. The mineralogy of the bulk samples was determined by XRD with CuKα radiation and a scanning speed of 1º2θ min^{-1} at the Turkish Petroleum Corporation (TPAO). Semi-quantitative abundances of rock-forming minerals were determined using sharp and

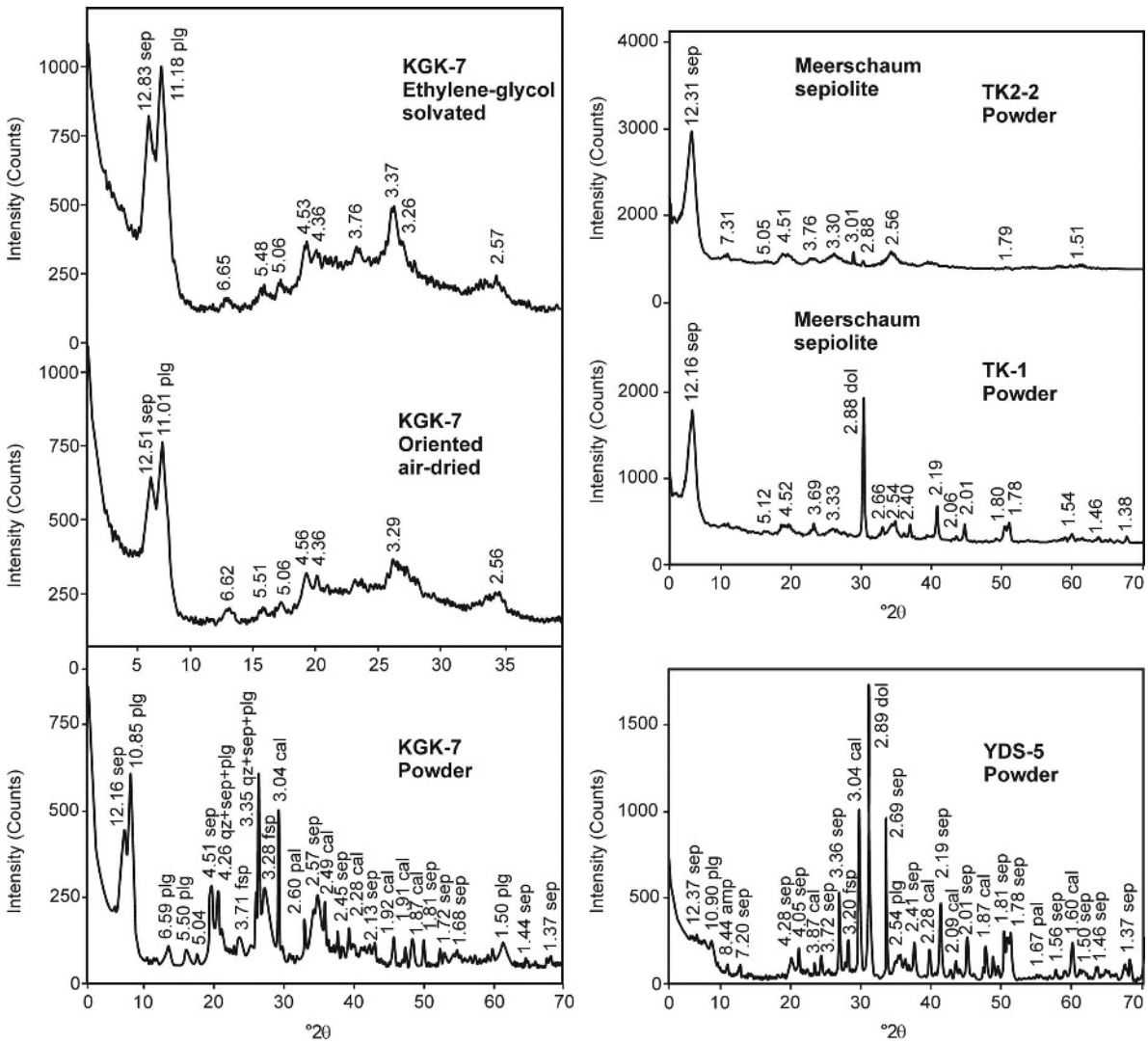

https://doi.org/10.1346/CCMN.2016.0640206 Published online by Cambridge University Press

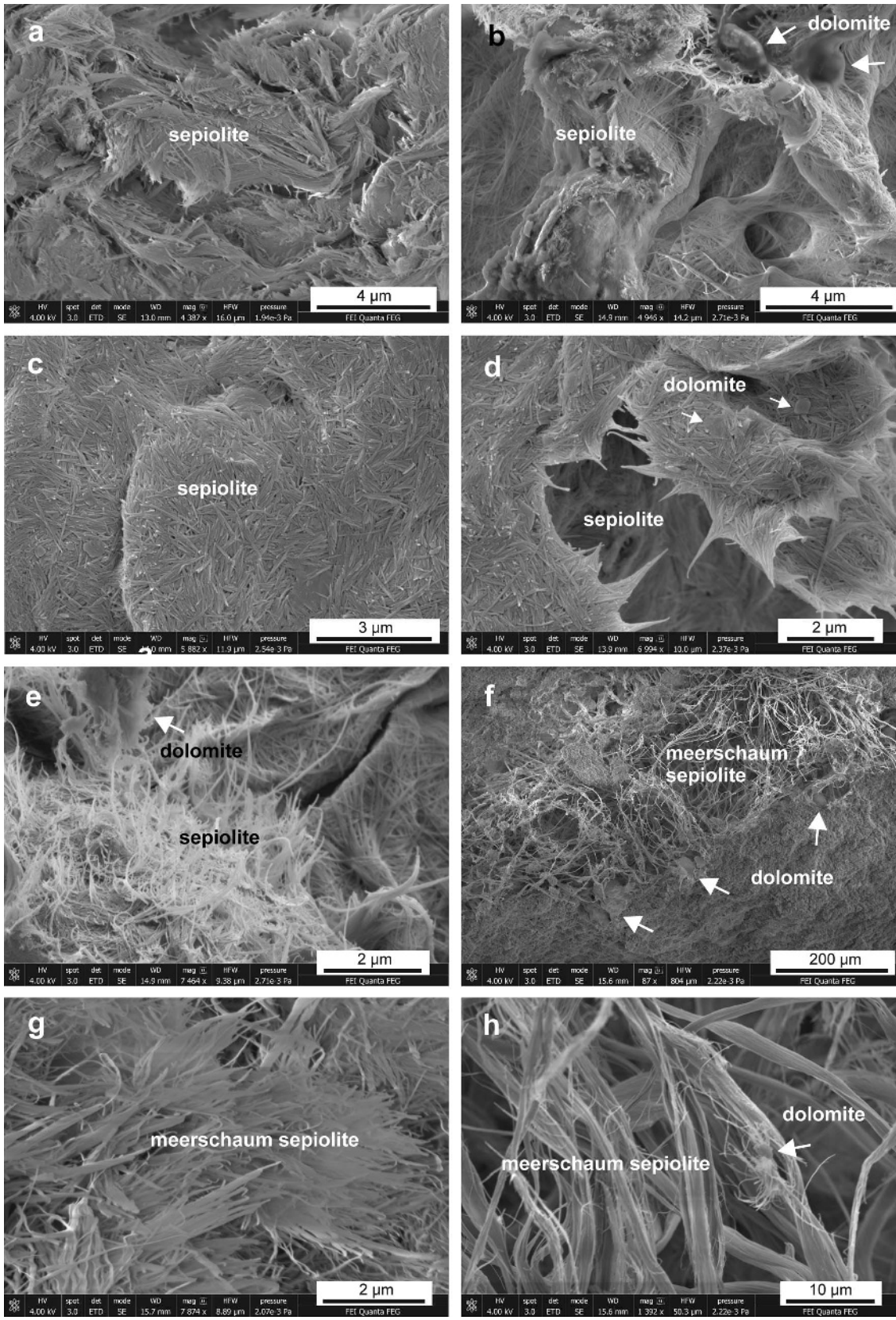

https://doi.org/10.1346/CCMN.2016.0640206 Published online by Cambridge University Press

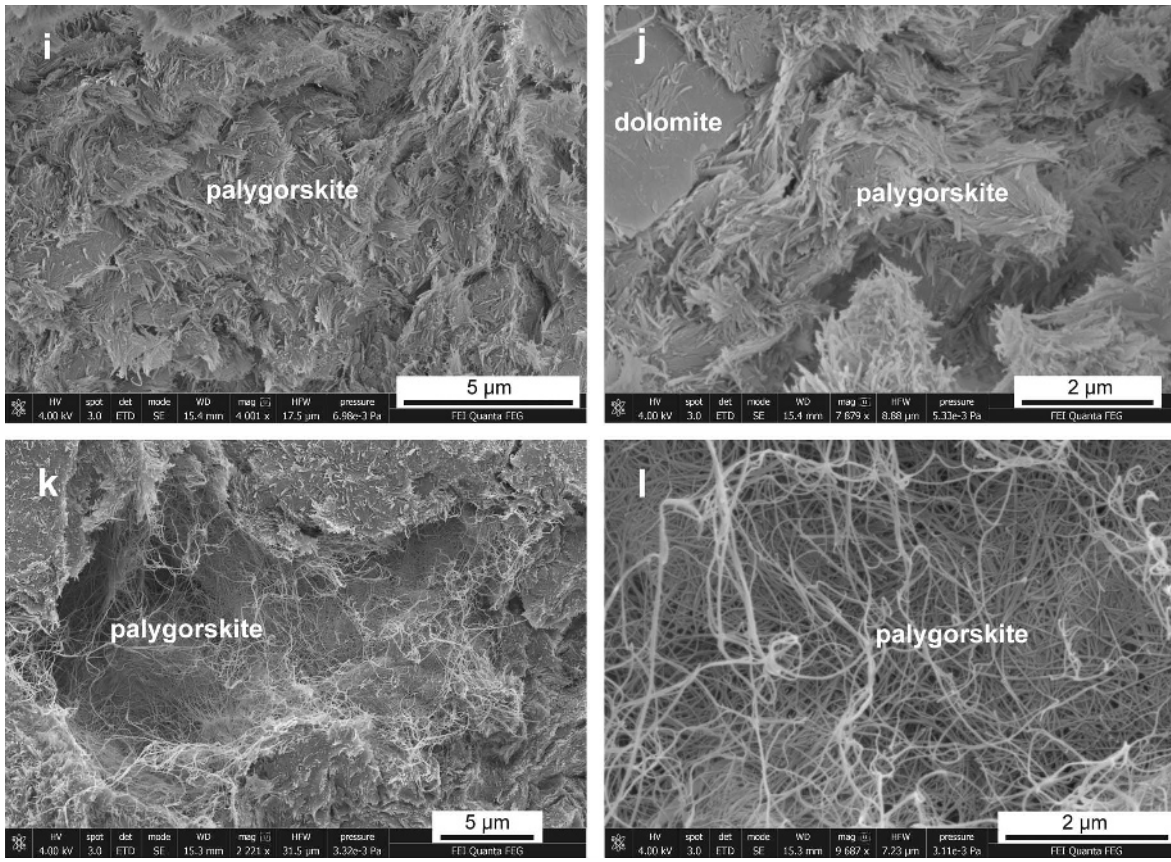

Figure 5 (*this and facing page*). SEM images showing: (a) sepiolite fiber bundles (OGL-4); (b) sepiolite fiber knit enclosing relics of carbonate grains (arrows) (OGL-4); (c) interwoven sepiolite fibers (OGL-4); (d) platy fan-like sepiolite with dolomite (arrows) (OGL-4); (e) scattered sepiolite fibers and fibers edging relics of dolomite (arrow) (OGL-4); (f) network form of meerschaum-type sepiolite edging relics of dolomite (arrows) and developed in microfracture (TK2-1); (g,h) oriented meerschaum type sepiolite enclosing relics of dolomite (arrow) (TK2-1); (i) massive interwoven palygorskite fibers (KGK-2); (j) palygorskite fibers enclosing dolomite rhombs (KGK-2); (k) interwoven palygorskite fibers grown in voids between platy fan-like palygorskite (KT2-13); (l) close-up view of k.

unambiguous diffraction peaks intensities on the XRD patterns (Brindley, 1980). The clay mineral relative abundances were determined from basal diffraction peaks and the mineral intensity factors of Moore and Reynolds (1989). Representative clay-dominated bulk samples were prepared for SEM-EDX analysis by adhering the fresh, broken surface of each sample onto an aluminum stub with double-sided tape and coating thinly (350 Å) with gold using a Giko ion coater at Oxford University, UK.

Whole-rock chemical analyses to determine major and trace elements were performed on 14 claystone and calcareous claystone samples at Acme Analytical Laboratories, Ltd. (Vancouver, Canada) using inductively coupled plasma–atomic emission spectroscopy (ICP–AES) (PerkinElmer Elan 9000, USA). The ICP-AES analyses were carried out on lithium metaborate/tetraborate fusions following dilute nitric acid digestion. The Spectro XLAB-2000 PEDX-ray fluorescence spectrometer was calibrated using USGS standards. Loss on ignition (LOI) was determined as the weight difference after ignition at 1000ºC. The detection limits for the analyses were between 0.01 and 0.1 wt.% for major elements, between 0.1 and 5 ppm for trace elements, and between 0.01 and 0.5 ppm for the rare earth elements (*REE*).

The composition and structural formulae of layer and meerschaum types of sepiolite and palygorskite were determined for the <2 µm clay fraction for samples with the highest sepiolite and palygorskite contents. Analyses were obtained using a JEOL JSM2000FX2 analytical transmission electron microscope (ATEM) with an Oxford instruments XMAXN 80 mm detector, and Oxford instruments INCA software for ATEM at the analytical facility at Imperial College, London, UK. This detector allows for very high count rates, and is, therefore, ideal for analyzing thin and small particles. A droplet of suspension was allowed to dry on a Cu grid coated with holey carbon. The analysis dwell time was 60 s and the beam current was 110 µA. The structural

https://doi.org/10.1346/CCMN.2016.0640206 Published online by Cambridge University Press

formulae of sepiolite and palygorskite were calculated on the basis of 32 and 21 oxygen atoms (Newman and Brown, 1987), respectively.

Nine sepiolite- and palygorskite-bearing clay fractions were purified for O and H stable isotope analysis at the Cornell Isotope Laboratory (Cornell University, New York, USA). Isotopic corrections were performed using a two-point normalization (regression), and referred to international standards IAEA CO-1 and IAEA CO-8 for $\delta^{18}O$ and CH-7 and benzoic acid for $\delta^{2}H$. The analyses were performed using a Thermo Delta V isotope ratio mass spectrometer interfaced with a temperature-conversion elemental analyzer. The delta values for ^{18}O and ^{2}H were measured against the primary reference scale of Clayton and Mayeda (1963). The data are reported in the standard delta notation as per-mil deviations from V-SMOW (Vienna Standard Mean Ocean Water). The external reproducibility for $\delta^{18}O$ was ±0.19‰ (1σ) based on repeated analyses of an internal white crystal standard consisting of benzoic acid. The NBS 28 value was 9.61 ± 0.10‰ (1σ).

RESULTS

XRD determinations

The semi-quantitative mineralogical compositions of samples collected from different lithologies in the study area were determined by X-ray diffraction (Table 1). Sepiolite, palygorskite, smectite, chlorite, dolomite, magnesite, calcite, as well as quartz, feldspar, and amphibole were identified. Sepiolite is abundant and associated mostly with dolomite, and locally with palygorskite and smectite, chlorite, magnesite, and calcite. Sepiolite nodules (meerschaum) have a high crystallinity, and are only rarely associated with dolomite.

Palygorskite predominates in the brown claystone and is relatively less abundant in the beige and white claystones (Figure 4). Locally, palygorskite is associated with sepiolite (e.g. samples YDS-5, KGK-5, KGK-6, KGK-7, and YSE-3). Palygorskite is associated with smectite in the Yörükakçayır region (samples YAC1-2, YAC1-4, YAC1-9, YAC2-3, YAC2-8, and YAC2-13). The abundance of dolomite ± magnesite ± calcite correlates with the whiteness of clayey units in dolomitic claystone or argilleous dolomite. In the basin as a whole, dolomite generally increases with decreasing sediment age, and at the Yukarı Dudaş village the dolomite is associated with accessory calcite, and locally with magnesite.

The sepiolite has a 110 peak of 12.16−12.58 Å, expanded to 12.83−12.87 Å with ethylene glycol treatment, and collapsed to 10.32 Å after heating to 550ºC for 2 h (Figure 4). The wide range of *d* spacing of sepiolite may characterize an intermediate form between Mg-sepiolite (meerschaum) and Al-sepiolite (Suárez and Garcia-Romero, 2011, 2013). The palygorskite has a 110 peak at 10.85−10.93 Å, expanded to 11.01−11.18 Å with ethylene-glycol solvation, and collapsed to 10.49 Å following heating to 550ºC for 2 h (Figure 4). The shift of the 110 reflection of this palygorskite to a higher value compared to that of ideal palygorskite at 10.5 Å might be due to the high Mg content of Mg-palygorskite (Suárez and Garcia-Romero, 2011, 2013). A slight increase in the XRD background of some of the sepiolite- and palygorskite-rich samples may indicate the presence of organic material.

SEM-EDX and TEM

Scanning electron microscope analyses were carried out on sepiolite-bearing samples, meerschaum sepiolite nodules, and palygorskite-bearing samples. Sepiolite and palygorskite fibers and fan-shaped fiber bundles were developed as sub-ordered, ordered, and interwoven textures or located on and between dissolved dolomite (Figure 5a-l). The development of oriented fibers and the absence of carbonate grains suggest direct precipitation under supersaturation conditions (Figure 5a-e). Sepiolite and palygorskite fibers in sepiolitic and palygorskitic claystone and sepiolite nodules (meerschaum) enclose relicts of dolomite rhombs (Figure 5b,d-f,h,j). The meerschaum sepiolite has longer, scattered, and subparallel fiber bundles and a more open meshwork fabric than the sepiolite in claystone. Sepiolite and palygorskite fibers have a shorter, more compact, massive interwoven, and knit morphology than meerschaum sepiolite (Figure 5a-l).

The EDX spectra of the claystone sepiolite fibers confirmed that it consists mainly of Si, plus Mg and Al; while the meerschaum sepiolite comprises Si and Mg with very little Al. Spectra for resorbed crystals between sepiolite and palygorskite fibers indicated that they are likely to be dolomite and magnesite.

Transmission electron microscopy confirms that sepiolite, sepiolite (meerschaum), and palygorskite particles consist of fibers, fiber bundles, and mesh networks (Figure 6a−d). Individual sepiolite and meerschaum fibers are thinner and longer than palygorskite crystals.

Chemical analyses

SiO_2, Al_2O_3, Fe_2O_3, MgO, CaO, and LOI contents for sepiolite- and palygorskite-bearing claystone and dolomitic claystone samples are variable, reflecting variable mineralogy (Table 2, Figures 1, 2). The claystone and calcareous claystone samples are characterized by SiO_2 (average 53.65 and 39.66 wt.%), MgO (average 16.04 and 15.16 wt.%), Al_2O_3 (average 6.16 and 5.49 wt.%), Fe_2O_3 (average 3.71 and 2.92 wt.%), CaO (average 1.02 and 8.85 wt.%), and LOI (average 17.40 and 26.09 wt.%) contents, respectively. The subparallel increase of MgO relative to CaO and LOI values in the calcareous claystone samples reflects the association of dolomite ± magnesite ± calcite with sepiolite and palygorskite.

https://doi.org/10.1346/CCMN.2016.0640206 Published online by Cambridge University Press

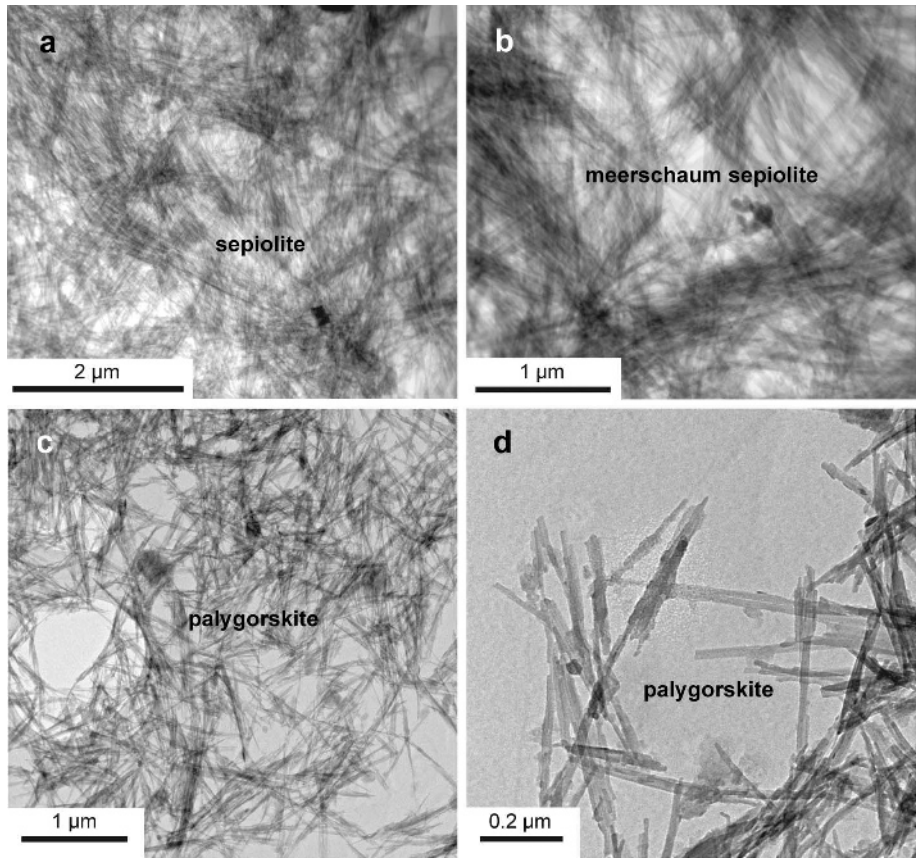

Figure 6. TEM images of fibrous sepiolite (OGL-4), meerschaum sepiolite (TK2-1), and palygorskite (KT2-13).

Al_2O_3 exhibits a negative correlation with MgO, and a positive correlation with Fe_2O_3+TiO_2 for claystone and dolomitic claystone samples, reflecting iron fixation into the structure of sepiolite and palygorskite (Figure 7). Al_2O_3 correlates positively with K_2O (0.1–1%), possibly due to the presence of accessory illite and feldspar. The Σ*REE vs.* Zr and Nb/Ti *vs.* La/Yb increase from the margin to the center of the basin (Figures 7, 8).

Ba, Rb, Nb, Ce, and Pr were depleted (Table 3; Figure 9). Weathering of K- and Ca-bearing minerals (such as feldspar) and hornblende resulted in the enrichment of Sr, and the leaching of Rb+Ba and K. Enrichment of Ni in claystone and calcareous claystone is related to weathering of ferromagnesian minerals such as olivine and pyroxene related to ophiolitic basement units.

The whole-rock *REE* contents were normalized to chondrite values and primitive mantle (Sun and McDonough, 1989; Figure 9). Light rare earth elements (*LREE*) are enriched relative to middle rare earth elements (*MREE*) and heavy rare earth elements (*HREE*), with negative Eu anomalies ($Eu/Eu^* = 0.71$).

The tetrahedral sites of both sepiolite and palygorskite are filled mainly by Si with trace Al substitution (Table 3). Mg is the dominant cation in octahedral sites in sepiolite; Mg+Al+Fe, in palygorskite. Al octahedral occupancy of 10.4 wt.% and cation content of 0.78 in Eskişehir sepiolite indicated that it is Al-sepiolite (Argast, 1989; Garcia-Romero and Suárez, 2010; Suárez and Garcia-Romero, 2011, 2013). The $MgO/(Al_2O_3+Fe_2O_3)$ ratio is 1.0 in Eskişehir palygorskite suggesting that this Mg-palygorskite is similar to the palygorskites reported by Garcia-Romero *et al.* (2004), Post and Crawford (2007), and Garcia-Romero and Suárez (2010). The tetrahedral site of meerschaum-type sepiolite is filled by Si. Mg is the dominant cation in the octahedral site, and only a trace of Fe substitutes for Mg, suggesting ideal, pure Mg-sepiolite (Galán and Carretero, 1999; Kadir *et al*., 2002; Suárez and Garcia-Romero, 2011).

Stable isotopes

The oxygen- and hydrogen-isotopic compositions of the sepiolite, meerschaum sepiolite, and palygorskite samples are listed in Table 4 and plotted in Figure 10. The $\delta^{18}O$ and δD values range between 9.32 and 33.83‰, and −88.99 and −64.70‰, respectively. These isotopic data fall on both sides of the kaolinite line (weathering) and the supergene–hypogene (S/H) line in equilibrium with meteoric water.

https://doi.org/10.1346/CCMN.2016.0640206 Published online by Cambridge University Press

Table 2. Major- (wt.%), and trace-element (ppm) compositions of the samples (see Table 1 for mineralogical compositions of the samples).

Claystone Major oxides (wt.%)	YAC-2	KT2-13	KGK-2	OGL-4	KI-6	YDN-1A	AHL-2	Average
SiO_2	48.91	51.50	55.00	53.50	52.88	57.41	56.32	53.65
Al_2O_3	7.60	9.53	9.39	8.79	0.83	5.32	1.67	6.16
ΣFe_2O_3	6.93	7.16	5.30	3.60	0.34	1.96	0.70	3.71
MgO	16.54	10.71	9.09	14.38	21.95	17.41	22.21	16.04
CaO	0.95	1.69	0.62	0.46	2.43	0.33	0.69	1.02
Na_2O	0.10	0.09	0.22	0.29	0.05	0.23	0.16	0.16
K_2O	0.81	1.63	1.56	1.55	0.16	0.94	0.30	0.99
TiO_2	0.45	0.56	0.51	0.54	0.04	0.28	0.08	0.35
P_2O_5	0.02	0.03	0.20	0.02	<0.01	0.03	<0.01	<0.06
MnO	0.07	0.06	0.05	0.02	<0.01	0.01	<0.01	<0.04
Cr_2O_3	0.199	0.129	0.071	0.043	<0.002	0.006	0.002	<0.08
LOI	17.0	16.7	17.8	16.3	20.9	15.7	17.4	17.40
Total	99.67	99.85	99.85	99.52	99.58	99.65	99.52	99.66
TOT/C	0.15	0.70	0.17	0.22	1.40	0.90	2.97	0.93
TOT/S	<0.02	<0.02	0.03	<0.02	0.03	0.04	0.30	<0.10
Trace elements (ppm)								
Ba	81	104	196	184	36	167	51	117
Be	<1	<1	2	2	<1	2	2	<2
Co	60.5	36.6	15.6	8.8	0.4	3.9	2.0	18.26
Cs	24.0	42.1	18.3	12.8	22.9	77.6	26.8	32.07
Ga	24.0	11.5	11.1	12.8	22.9	77.6	26.8	26.67
Hf	2.3	2.8	2.7	2.6	0.4	1.9	0.7	1.91
Nb	9.0	29.2	11.6	11.2	1.6	6.7	1.8	10.16
Ni	950	747	268	82	<20	<20	<20	<511.75
Rb	48.5	115.2	111.8	69.4	14.2	70.0	21.6	64.39
Sc	14	15	14	9	<1	5	1	<9.67
Sn	1	2	2	1	<1	<1	<1	<1.5
Sr	74.6	74.5	81.4	81.8	542.6	87.1	807.4	249.91
Ta	0.8	1.3	0.8	0.7	0.1	0.8	0.1	0.66
Th	5.9	9.2	9.6	6.2	0.7	4.0	2.5	5.44
U	0.9	1.1	2.5	1.8	5.4	2.6	7.0	3.04
V	105	71	218	1058	51	147	92	248.86
W	0.9	0.9	1.6	0.8	<0.5	0.6	2.2	<1.17
Zr	85.2	113.3	113.6	98.1	11.6	65.6	24.5	73.13
Y	6.1	9.7	19.9	5.8	1.5	6.2	2.4	7.37
La	13.6	27.9	24.9	11.5	2.5	13.7	4.9	14.14
Ce	33.4	42.2	41.1	20.2	5.2	25.0	9.3	25.20
Pr	2.83	4.66	5.09	2.23	0.45	2.84	0.93	2.72
Nd	10.8	16.7	18.8	7.4	2.0	10.9	3.3	9.99
Sm	1.89	3.17	3.78	1.55	0.36	1.85	0.66	1.89
Eu	0.39	0.59	0.85	0.27	0.06	0.40	0.12	0.38
Gd	1.54	2.20	3.46	1.25	0.36	1.56	0.52	1.56
Tb	0.22	0.33	0.52	0.19	0.04	0.22	0.07	0.23
Dy	1.19	2.00	3.39	1.15	0.20	1.34	0.41	1.38
Ho	0.20	0.36	0.66	0.21	0.04	0.22	0.07	0.25
Er	0.71	1.05	1.84	0.77	0.18	0.73	0.22	0.79
Tm	0.10	0.16	0.30	0.11	0.02	0.09	0.03	0.12
Yb	0.66	1.16	2.13	0.76	0.11	0.69	0.19	0.81
Lu	0.09	0.17	0.34	0.12	0.01	0.10	0.03	0.12
Mo	<0.1	<0.1	<0.1	<0.1	0.1	<0.1	0.5	<0.30
Cu	25.5	20.6	37.4	20.1	0.8	5.2	1.6	15.89
Pb	4.7	10.2	9.3	8.3	1.2	5.2	4.4	6.19
Zn	55	51	47	44	6	23	26	36
As	6.4	1.6	5.2	5.4	6.3	5.8	10.7	5.91
Cd	<0.1	0.2	<0.1	<0.1	<0.1	<0.1	<0.1	<0.2
Sb	<0.1	<0.1	0.7	0.5	0.6	0.1	0.5	<0.48
Bi	0.2	0.2	0.2	0.2	<0.1	<0.1	<0.1	<0.2
Ag	<0.1	<0.1	<0.1	0.6	<0.1	<0.1	<0.1	<0.6

https://doi.org/10.1346/CCMN.2016.0640206 Published online by Cambridge University Press

Table 2 (*contd.*)

Claystone Trace elements (ppm)	YAC-2	KT2-13	KGK-2	OGL-4	KI-6	YDN-1A	AHL-2	Average
Au	1.7	1.5	3.1	1.8	<0.5	0.7	0.6	<1.57
Hg	<0.01	<0.01	0.01	0.03	<0.01	0.02	0.05	<0.03
Tl	0.2	0.3	0.3	0.2	0.1	0.1	0.2	0.2
Se	<0.5	<0.5	<0.5	<0.5	<0.5	<0.5	1.6	<1.6
Σ*REE*	73.72	112.35	127.06	53.51	13.03	65.84	23.15	66.95
Σ*LREE*	60.63	91.46	89.89	41.33	10.15	52.44	18.43	52.05
Σ*MREE*	5.43	8.65	12.66	4.62	1.06	5.59	1.85	5.69
Σ*HREE*	1.56	2.54	4.61	1.76	0.32	1.61	0.47	1.84

Calcareous claystone Major oxides (wt.%)	YAC2-8	KGK-5	KGK-7	TK2-3	GNU-1	YSE-3	IL-15	Average
SiO_2	40.06	37.09	47.76	39.58	29.38	43.47	40.31	39.66
Al_2O_3	8.24	5.96	7.51	0.07	7.96	6.78	1.94	5.49
ΣFe_2O_3	4.88	3.49	4.17	0.08	3.20	3.92	0.67	2.92
MgO	15.05	13.27	8.93	30.09	6.76	12.32	19.71	15.16
CaO	5.35	11.06	6.76	1.31	21.69	6.68	9.09	8.85
Na_2O	0.10	0.21	0.15	<0.01	0.44	0.15	0.30	<0.23
K_2O	1.38	0.89	1.14	<0.01	1.63	1.16	0.28	<1.08
TiO_2	0.43	0.38	0.41	<0.01	0.37	0.40	0.11	<0.35
P_2O_5	0.04	0.04	0.24	<0.01	0.08	0.07	<0.01	<0.09
MnO	0.06	0.10	0.03	<0.01	0.06	0.04	<0.01	<0.06
Cr_2O_3	0.072	0.028	0.051	0.016	0.009	0.052	0.002	0.03
LOI	23.9	27.3	22.7	28.7	28.2	24.7	27.1	26.09
Total	99.64	99.85	99.83	99.96	99.75	99.78	99.51	99.76
TOT/C	2.11	4.99	1.76	4.23	5.65	3.47	4.02	3.75
TOT/S	<0.02	<0.02	<0.02	<0.02	0.03	<0.02	0.15	<0.09
Trace elements (ppm)								
Ba	107	246	155	3	168	234	95	144
Be	<1	<1	2	<1	2	<1	<1	<2
Co	24.0	17.4	13.8	1.3	10.5	10.9	5.2	11.87
Cs	52.2	7.8	16.1	<0.1	5.4	21.1	27.1	<21.62
Ga	9.7	7.1	9.3	<0.5	5.4	7.5	1.8	<6.8
Hf	2.5	2.1	2.3	<0.1	2.0	2.1	0.8	<1.97
Nb	11.9	8.1	10.6	<0.1	8.6	7.9	3.0	<8.35
Ni	489	122	163	638	55	182	23	238.86
Rb	96.9	65.8	85.7	<0.1	61.8	85.3	20.1	<69.27
Sc	10	8	10	<1	7	11	2	<8
Sn	2	<1	1	<1	<1	1	<1	<1.33
Sr	333.9	352.1	316.3	20.9	659.0	997.0	1291.1	567.19
Ta	1.0	0.5	0.6	<0.1	0.6	0.5	0.1	<0.55
Th	10.5	5.1	6.9	<0.2	6.1	12.6	1.3	<7.08
U	1.7	1.3	1.6	<0.1	4.6	1.7	2.5	<2.23
V	67	98	196	<8	69	98	44	<95.33
W	1.3	1.8	1.4	<0.5	0.8	1.8	<0.5	<1.42
Zr	93.5	79.4	89.9	1.0	82.1	80.2	24.6	64.39
Y	12.4	10.9	14.6	0.3	9.8	12.3	2.0	8.9
La	20.9	14.6	19.3	0.5	18.0	25.8	4.3	14.77
Ce	39.4	27.7	35.9	0.2	33.8	44.0	7.4	26.91
Pr	4.12	3.02	3.91	<0.02	3.65	4.91	0.71	<3.39
Nd	14.5	11.3	14.4	<0.3	13.7	17.5	2.9	<12.38
Sm	2.71	2.22	2.73	<0.05	2.63	3.31	0.52	<2.35
Eu	0.53	0.51	0.67	<0.02	0.57	0.81	0.08	<0.53
Gd	2.67	2.08	2.79	<0.05	2.21	3.01	0.43	<2.2
Tb	0.42	0.33	0.41	<0.01	0.35	0.45	0.05	<0.34
Dy	2.61	1.94	2.27	<0.05	1.93	2.39	0.35	<1.92
Ho	0.51	0.39	0.46	<0.02	0.37	0.47	0.06	<0.38
Er	1.39	1.14	1.45	<0.03	1.10	1.30	0.25	<1.11

https://doi.org/10.1346/CCMN.2016.0640206 Published online by Cambridge University Press

Table 2 (*contd.*)

Calcareous claystone Trace elements (ppm)	YAC2-8	KGK-5	KGK-7	TK2-3	GNU-1	YSE-3	IL-15	Average
Tm	0.22	0.16	0.20	<0.01	0.15	0.19	0.03	<0.16
Yb	1.50	0.96	1.37	<0.05	1.00	1.30	0.20	<1.06
Lu	0.23	0.17	0.21	<0.01	0.15	0.18	0.03	<0.16
Mo	<0.1	0.3	<0.1	<0.1	0.7	0.2	0.2	<0.35
Cu	22.0	25.1	24.2	3.3	12.7	21.1	6.9	16.47
Pb	10.7	10.0	11.0	0.1	9.2	5.2	1.1	6.76
Zn	44	30	39	12	43	34	11	30.43
As	16.9	5.8	5.5	<0.5	7.4	4.9	6.7	<7.87
Cd	0.1	0.3	<0.1	<0.1	<0.1	<0.1	<0.1	<0.2
Sb	<0.1	0.7	0.5	<0.1	<0.1	0.2	0.3	<0.43
Bi	0.2	0.1	0.2	<0.1	0.1	0.1	<0.1	<0.14
Ag	<0.1	<0.1	<0.1	<0.1	<0.1	0.5	<0.1	<0.5
Au	0.6	40.8	5.8	2.7	1.2	2.6	0.8	7.79
Hg	<0.01	0.01	<0.01	<0.01	<0.01	0.85	0.02	<0.29
Tl	0.3	0.2	0.3	<0.1	0.1	0.3	<0.1	<0.24
Se	<0.5	<0.5	<0.5	<0.5	<0.5	<0.5	<0.5	<0.5
Σ*REE*	104.11	77.42	100.67	<1.62	89.41	117.92	19.31	<84.81
Σ*LREE*	78.92	56.62	73.51	<1.02	69.15	92.21	15.31	<64.29
Σ*MREE*	9.45	7.47	9.33	<0.2	8.06	10.44	1.49	<7.71
Σ*HREE*	3.34	2.43	3.23	<0.1	2.4	2.97	0.51	<2.48

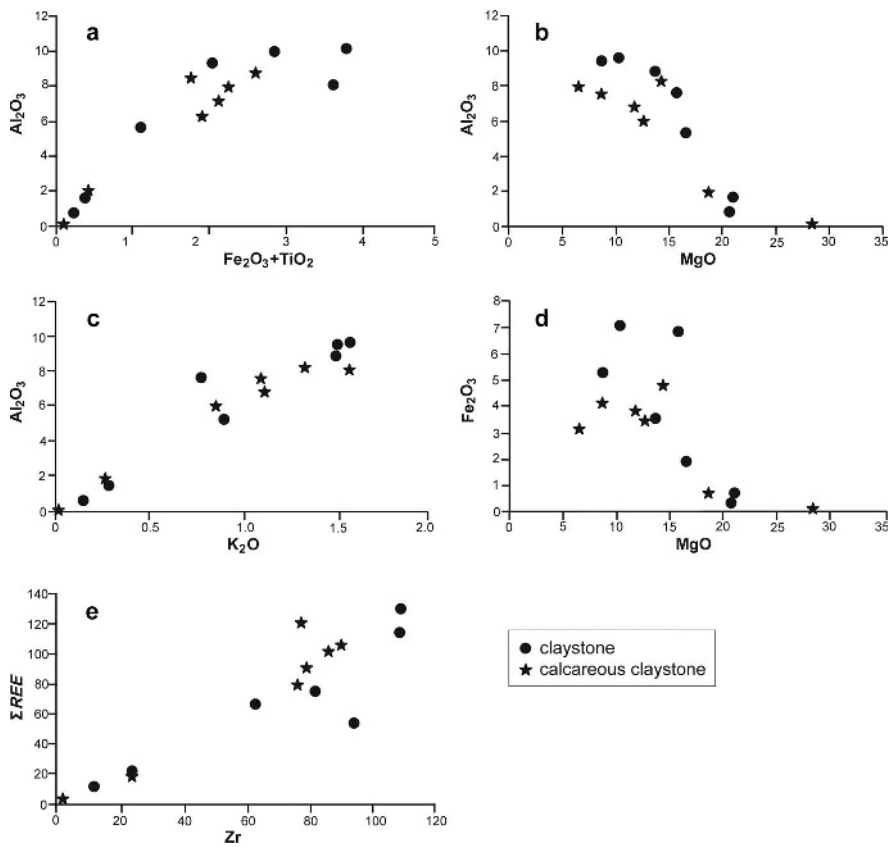

Figure 7. Elemental variation diagrams for major oxides (wt.%) and trace elements (ppm) of the claystone and calcareous claystone samples. (a) Al_2O_3 *vs.* $Fe_2O_3 + TiO_2$; (b) Al_2O_3 *vs.* MgO; (c) Al_2O_3 *vs.* K_2O; (d) Fe_2O_3 *vs.* MgO; (e) Σ*REE vs.* Zr.

https://doi.org/10.1346/CCMN.2016.0640206 Published online by Cambridge University Press

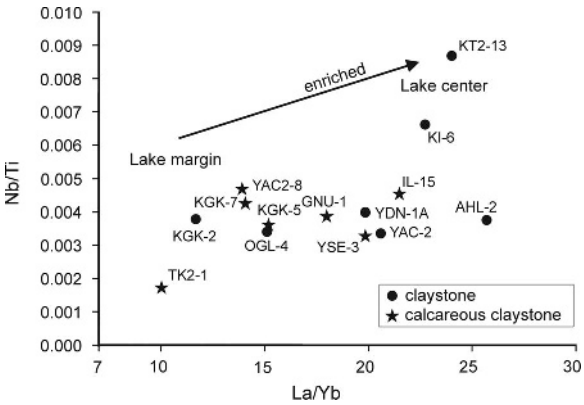

Figure 8. Plots of La/Yb *vs*. Nb/Ti for the sepiolite- and palygorskite-dominated claystone and calcareous claystone samples of the study area.

DISCUSSION

The lake basins in the Eskişehir province were developed by extensional faulting. Widespread precipitation of sepiolite and palygorskite beds occurred, together with dolomite, in a shallow-lacustrine environment during the Late Miocene to Early Pliocene (Figure 11). These beds are overlain by detrital sediment derived from ophiolitic and carbonate units deposited during the wet season. The detritus includes organic-rich materials, locally sufficiently abundant to form lignite. Gypsum-bearing green claystone developed along faults. The alternation of claystone, calcareous claystone, and marls reflects the periodic climatic changes. The sediments show vertical and lateral changes in lithology and in mineralogical and chemical composition.

Sepiolite and palygorskite occur in claystone and marl beds, locally intercalated with organic-matter-bearing brown to black claystone lenses. An increase in dolomite and argillaceous dolomite occurs up section, and an increase in organic-material-bearing sepiolite and palygorskite lenses occurs toward the base of the section. The lithological association is interpreted as having been deposited in shallow playa lakes with localized swamp environments. An increase in carbonate content up section indicates an environment of supersaturation caused by near-surface evaporation of solutions, resulting in the precipitation of dolomite (Wright, 1984). This interpretation is consistent with the precipitation of widespread massive, brown, and black sepiolite associated with beige dolomitic sepiolite and sepiolitic dolomite. This occurred through extensive biogenic activity and humic acid production, deepening

Table 3. Chemical compositions (wt.%) and structural formulae of sepiolite, meerschaum sepiolite, and palygorskite obtained from ATEM analyses.

	Sepiolite			Meerschaum sepiolite			Palygorskite			
Major oxides (wt%)	OGL-4	YDN-1	avg.	TK2-1	TK2-2	avg.	KGK-2	KT2-13	YSE-1	avg.
SiO_2	68.27	69.01	68.64	69.01	69.12	69.07	67.00	66.10	68.90	67.33
Al_2O_3	4.92	3.52	4.22	0.00	0.00	0.00	10.20	10.60	9.90	10.23
ΣFe_2O_3	1.72	0.23	0.98	0.08	0.14	0.11	5.20	4.40	3.50	4.37
MgO	24.23	26.80	25.52	30.80	29.88	30.34	14.80	13.70	15.60	14.70
CaO	0.00	0.00	0.00	0.00	0.00	0.00	1.00	1.10	0.80	0.97
Na_2O	0.44	0.25	0.35	0.00	0.76	0.38	0.80	2.80	0.70	1.43
K_2O	0.38	0.18	0.28	0.09	0.17	0.13	1.00	1.20	0.60	0.93
SiO_2/Al_2O_3	13.88	19.61	16.75	–	–	–	6.57	6.24	6.96	6.59
Tetrahedral										
Si	11.87	11.95	11.91	12.00	12.03	12.02	7.71	7.67	7.85	7.74
Al	0.13	0.05	0.09	0.00	0.00	0.00	0.29	0.33	0.15	0.26
Σ	12.00	12.00	12.00	12.00	12.03	12.02	8.00	8.00	8.00	8.00
Octahedral										
Al	0.88	0.67	0.78	0.00	0.00	0.00	1.10	1.12	1.17	1.13
Mg	6.28	6.92	6.60	7.98	7.76	7.87	2.54	2.37	2.65	2.52
Fe	0.22	0.03	0.13	0.01	0.02	0.01	0.45	0.38	0.30	0.38
Σ	7.38	7.63	7.51	7.99	7.78	7.88	4.09	3.87	4.12	4.03
Interlayer										
Ca	0.00	0.00	0.00	0.00	0.00	0.00	0.12	0.14	0.10	0.12
Na	0.15	0.08	0.12	0.00	0.26	0.13	0.18	0.63	0.16	0.32
K	0.08	0.04	0.06	0.02	0.04	0.03	0.15	0.18	0.09	0.14
Σ	0.23	0.12	0.18	0.02	0.30	0.16	0.45	0.95	0.35	0.58
Tetrahedral charge	0.13	0.05	0.09	0.00	-0.14	-0.07	0.29	0.33	0.16	0.26
Octahedral charge	0.10	0.07	0.09	0.01	0.43	0.22	0.28	0.75	0.28	0.44
Total charge	0.23	0.12	0.18	0.01	0.29	0.15	0.57	1.08	0.44	0.70
Interlayer charge	0.23	0.12	0.18	0.02	0.29	0.16	0.57	1.08	0.44	0.70

https://doi.org/10.1346/CCMN.2016.0640206 Published online by Cambridge University Press

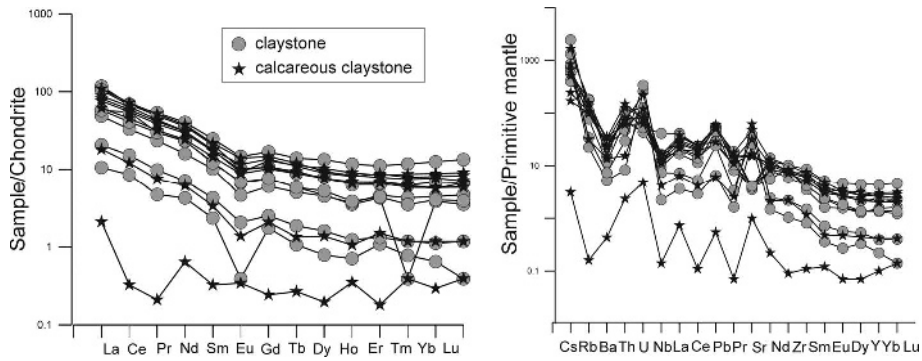

Figure 9. Chondrite and primitive mantle-normalized (Sun and McDonough, 1989) patterns for claystone and calcareous claystone samples from the Eskişehir regions.

of the swamp, and the formation of a longer-lived dolomitic playa lake in the marginal and deepest zones.

Lateral mineralogical zonation from the shallow margin to an open lake eastward is as follows: smectite ± palygorskite ± sepiolite; palygorskite + sepiolite ± smectite; sepiolite ± dolomite; and sepiolite + dolomite ± gypsum (Figure 11). Dolomite and gypsum imply precipitation in a shallow-water environment under arid climatic conditions. Smectite associated with palygorskite in the Yörükakçayır region may be saponitic smectite derived from Mg-rich ophiolitic basement rocks. Palygorskite formed by direct precipitation with increasing Al/Mg ratios in the fluid environment rather than at the lake margin (Singer and Norrish, 1974; Colson *et al*., 1998).

Microscopically, the development of sepiolite and palygorskite as massive interwoven fibers, fans, and knitted aggregates of fiber bundles, plus an absence of dolomite, indicate direct precipitation from supersaturated solution. Fibers edging dolomite crystals indicate that both sepiolite and palygorskite formation post-dated dolomite, and occurred by precipitation under semi-arid to arid climatic conditions. Development of palygorskite fibers on dolomite rhombs is also consistent with authigenic origin.

A decrease of the Ca/Mg ratio during precipitation of carbonates and gypsum in the marginal zone, and after dolomitization resulting from evaporation, in the inner zones, and adequate Si^{4+} concentration, all favored precipitation and/or coprecipitation of Al-sepiolite and Mg-palygorskite, respectively (Garcia-Romero and Suárez, 2010; Suárez and Garcia-Romero, 2011, 2013). These clays have average structural formulae of $Si_{11.91}Al_{0.09}O_{30}Mg_{6.60}Al_{0.78}Fe_{0.13}(OH)_4Na_{0.12}K_{0.06}(OH_2)_4{\cdot}nH_2O$ and $Si_{7.74}Al_{0.26}O_{20}Mg_{2.52}Al_{1.13}Fe_{0.38}(OH)_2(OH_2)_4Na_{0.32}K_{0.14}Ca_{0.12}{\cdot}nH_2O$, respectively. The above hypothesis for the clay origins is consistent with the alternation of sepiolitic- and palygorskitic-dolomite, dolomitic-sepiolite and -palygorskite, sepiolite, palygorskite, and dolomite layers through the partial drying of the alkaline lakes located in the central region, far from the basement rocks.

An increase in Mg and Si (and the absence of Al) concentrations in the percolating fluid(s) in ophiolitic materials of the Beyazaltın, Türkmentokat, and Nemli regions favored the formation of meerschaum Mg-sepiolite from pre-existing magnesite gravels by a dissolution/precipitation mechanism in an alkaline environment (Yeniyol, 1986; Ece and Çoban, 1994) near the margin of the basin. This is evidenced by

Table 4. Oxygen and hydrogen isotopic compositions of sepiolite, meerschaum sepiolite, and palygorskite in the Eskişehir area.

Sample ID	Mineralogy	Weight (mg)	H (wt.%)	Normalized δ^2H *vs.* VSMOW	Weight (mg)	O (wt.%)	Normalized $\delta^{18}O$ *vs.* VSMOW
YSE-8	sepiolite	1.53	0.51	−88.99	1.527	26.31	26.27
OGL-7	sepiolite	1.51	0.25	−86.45	1.522	33.40	33.83
KI-8	sepiolite	1.50	1.06	−75.64	1.481	11.13	9.32
IL-15	sepiolite	1.56	0.41	−79.40	1.518	28.33	24.91
VEL1-7	sepiolite	1.56	0.74	−73.55	1.503	14.60	17.15
YDN-3	sepiolite	1.51	0.53	−87.92	1.544	25.11	24.33
TK2-2	meerschaum sepiolite	1.54	1.07	−81.75	1.516	14.62	11.50
KT2-13	palygorskite	1.50	1.07	−64.70	1.520	12.50	11.15
KGK-7	palygorskite	1.53	0.89	−66.71	1.513	16.64	14.79

https://doi.org/10.1346/CCMN.2016.0640206 Published online by Cambridge University Press

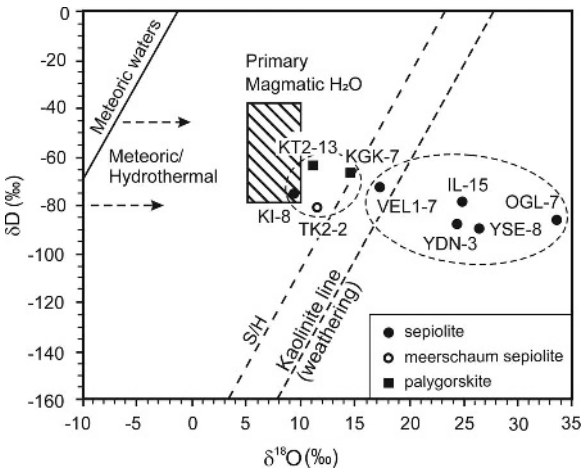

Figure 10. $\delta^{18}O$ *vs*. δD plot (Sheppard, 1986) showing isotopic compositions of sepiolite, meerschaum sepiolite, and palygorskite from the Eskişehir region. The kaolinite line is from Savin and Epstein (1970); S/H, supergene/hypogene kaolinite equilibrium line with meteoric water at 35ºC is from Sheppard *et al.* (1969). The meteoric water line is from Craig (1961).

magnesite remnants at the centers of some meerschaum sepiolite nodules (Ece and Çoban, 1994). The structural formula of the meerschaum sepiolite is $Si_{12.02}O_{30}Mg_{7.87}Fe_{0.01}(OH)_4Na_{0.13}K_{0.03}(OH_2)_4{\cdot}nH_2O$.

The southeastward increase of Mg+Fe+Ni, Sr, *LREE*/(*MREE*+*HREE*), La/Yb, Nb/Ti, and Zr ratios, the leaching of Rb+Ba and K, and the small negative Eu anomalies, suggest that Mg required for dolomitization and Mg+Al for precipitation of sepiolite and palygorskite were supplied in fluid(s) from degradation of olivine and pyroxene derived from ophiolitic basement units and from feldspar and amphibole derived from volcanic units (Kadir *et al*., 2002; Figure 11).

The isotopic data for sepiolite from Sivrihisar basinward fall to the right of the S/H 35ºC line (Figure 10) indicating its contribution from equilibration with meteoric water and low-temperature chemical weathering processes (Craig, 1961; Lawrence and Taylor, 1971, 1972; Taylor, 1974). In contrast, palygorskite formed in the west and north sides of the basin plots between S/H and the primary magmatic field, in equilibrium with meteoric water (Taylor, 1974, 1979). This implies that the formation of the Eskişehir sepiolite can be attributed to alteration by meteoric water, the availability of which was, in turn, controlled by climatic conditions. Additionally, palygorskite and meerschaum sepiolite shift to lower $\delta^{18}O$ and slightly higher δD values, near the magmatic "box," so their formation may have been influenced by hydrothermal heating of meteoric waters during the alteration processes along overthrust fault zones at the west and north of the study area (Faure, 1986). This mechanism is consistent with the calculated formation temperature (187–416ºC) for the tectonically controlled Eskişehir tremolite and

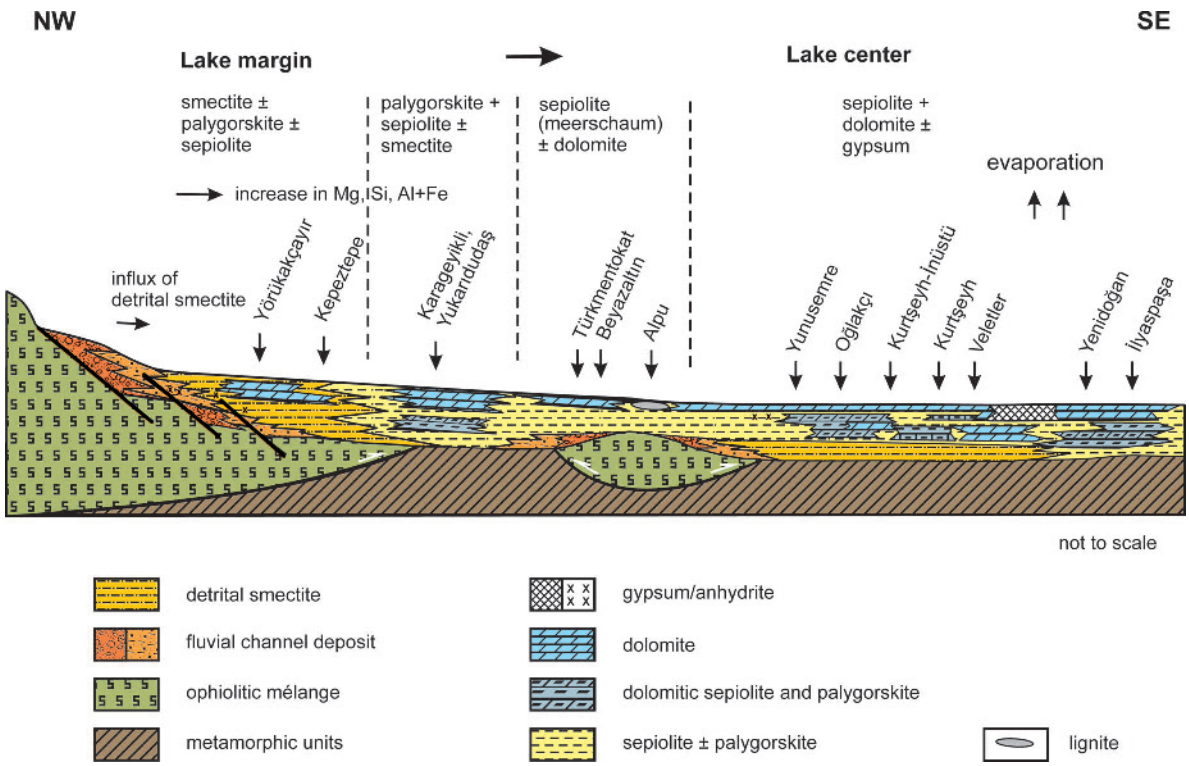

Figure 11. Genetic model for the Eskişehir sepiolite and palygorskite deposits.

https://doi.org/10.1346/CCMN.2016.0640206 Published online by Cambridge University Press

chrysotile deposits based on O and H isotope data (Kadir and Erkoyun, 2015) and the occurrence of hot springs along faults exhibiting reservoir temperatures of (73–200ºC) in the Eskişehir region based on silica geothermometry, quartz, and chalcedony solubility (Yüce *et al*., 2015).

CONCLUSIONS

Field observations and mineralogical and geochemical analyses reveal that Al-sepiolite and Mg-palygorskite of the Eskişehir Neogene basin (west central Anatolia) developed mainly during the Late Miocene to Early Pliocene, in large lakes, that, critically for sepiolite formation, were surrounded by swamps, peat (that became coal), and evaporites. This basin was supplied with sediment and cations in solution from nearby volcanoes, and from uplifted older sedimentary, ophiolitic, and metamorphic rocks. The alternation of Al-sepiolitic and Mg-palygorskitic claystone, dolomitic sepiolite, and palygorskite and dolomite suggest alkaline, shallow, swampy lacustrine depositional conditions, with the alternation being controlled by periodic climatic changes and changes in the Mg±Al/Si ratio.

Meerschaum-type Mg-sepiolite deficient in Al indicates the precipitation of Mg-sepiolite from Mg-rich fluids under alkaline physicochemical environmental conditions, with local redeposition as clasts within fluvial deposits. The plot of $\delta^{18}O$ and δD values for sepiolite and palygorskite on either side of both the kaolinite values and the S/H lines suggest the influx of meteoric lacustrine fluid phases and hydrothermal processes.

ACKNOWLEDGMENTS

This study was supported financially by the Scientific Research Projects Fund of Eskişehir Osmangazi University in the framework of Project 2014–487. The authors are much indebted to anonymous reviewers for their extremely careful and constructive reviews which improved the quality of the paper significantly. They are also extremely grateful to an anonymous Associate Editor, Editor in Chief, Joseph W. Stucki, Acting Editor in Chief, Michael A. Velbel, and Managing Editor, Kevin Murphy for their insightful editorial comments and suggestions. Tacit Külah is also thanked for his assistance during the drafting of the figures. This paper was presented at Euroclay 2015, held at Edinburgh University, Scotland.

REFERENCES

Akbulut, A. and Kadir, S. (2003) The geology and origin of sepiolite, palygorskite and saponite in Neogene lacustrine sediments of the Serinhisar-Acıpayam basin, Denizli, SW Turkey. *Clays and Clay Minerals*, **51**, 279–292.

Akıncı, Ö. (1967) Eskişehir İ24 c1 paftasının jeolojisi ve tabakalı lületaşı zuhurları. *MTA Enstitüsü Dergisi*, **68**, 82–97.

Argast, S. (1989) Expandable sepiolite from Ninetyeast Ridge, Indian Ocean. *Clays and Clay Minerals*, **37**, 371–376.

Bilgen, A.N. (2006) Çavlum Orta Tunç Çağı Nekropolü'nde ele geçen lületaşı mühür. *Elektronik Sosyal Bilimler Dergisi*, **16**, 17–21.

Brindley, G.W. (1980) Quantitative X-ray analysis of clays. Pp. 411–438 in: *Crystal Structures of Clay Minerals and their X-ray Identification* (G.W. Brindley and G. Brown, editors). Mineralogical Society Monograph **5**, London.

Clayton, R.N. and Mayeda, T.K. (1963) The use of bromine pentafluoride in the extraction of oxygen from oxides and silicates for isotopic analysis. *Geochimica et Cosmochimica Acta*, **27**, 43–52.

Colson, J., Cojan, I., and Thiry, M. (1998) A hydrogeological model for palygorskite formation in the Danian continental facies of the Provence Basin (France). *Clay Minerals*, **33**, 333–347.

Craig, H. (1961) Isotopic variations in meteoric waters. *Science*, **133**, 1702–1703.

Ece, Ö.I. (1998) Diagenetic transformation of magnesite pebbles and cobbles to sepiolite (Meerschaum) in Eskişehir lacustrine basin, Turkey. *Clays and Clay Minerals*, **46**, 436–445.

Ece, Ö.I. and Çoban, F. (1994) Geology, occurrence, and genesis of Eskişehir sepiolites, Turkey. *Clays and Clay Minerals*, **42**, 81–92.

Eren, M., Kadir, S., Hatipoğlu, Z., and Gül, M. (2004) Caliche development in Mersin area. TÜBİTAK Project, No.102Y036,136 pp. (In Turkish with English abstract).

Eren, M., Kadir, S., Hatipoğlu, Z., and Gül, M. (2008) Quaternary calcrete development in the Mersin area, southern Turkey. *Turkish Journal of Earth Sciences*, **17**, 763–784.

Faure, G. (1986) *Principles of Isotope Geology*, 2nd edition, John Wiley & Sons, New York, 589 pp.

Fukushima, Y. and Shimosaka, K. (1987) Sepiolite deposit in central Anatolia, Turkey. Summaries – Proceedings of the 6th Meeting of the European Clay Groups, Sevilla, pp. 226–228.

Galán, E. and Carretero, M.I. (1999) A new approach to compositional limits for sepiolite and palygorskite. *Clays and Clay Minerals*, **47**, 399–409.

Galán, E. and Ferrero, A. (1982) Palygorskite-sepiolite clays of Lebrija, southern Spain. *Clays and Clay Minerals*, **30**, 191–199.

Galán, E. and Pozo, M. (2011) Palygorskite and sepiolite deposits in continental environments. Description, Genetic Patterns and Sedimentary Settings. Pp. 125–173 in: *Developments in Palygorskite-Sepiolite Research. A New Outlook on these Nanomaterials* (E. Galán and E. Singer, editors). Developments in Clay Science, Vol. **3**. Elsevier, Amsterdam.

Garcia-Romero, E., Suárez Barrios, M., and Bustillo Revuelta, A. (2004) Characteristics of a Mg-palygorskite in Miocene rocks, Madrid Basin (Spain). *Clays and Clay Minerals*, **52**, 484–494.

Garcia-Romero, E. and Suárez, M. (2010) On the chemical composition of sepiolite and palygorskite. *Clays and Clay Minerals*, **58**, 1–20.

Gençoğlu, H. (1996) Eskişehir-Sivrihisar-Oğlakçı köyü sepiyolit sahasına ait maden jeolojisi. MTA Raport No. 9858, Ankara, 33s (unpublished).

Gözler, M.Z., Cevher, F., Ergül, E., and Asutay, H.J. (1996) Orta Sakarya ve güneyinin jeolojisi, Mineral Research and Exploration (MTA) Raport No. 9973 (unpublished).

İrkeç, T. (1987–1988) General geological setting and character of Turkish sepiolite deposits. *Acta Mineralogica-Petrographica*, **XXIX**, 95–106.

İrkeç, T. and Gençoğlu, H. (1993) Eskişehir, Sivrihisar, Sığırcık, Kurtşeyh köyleri ÖIR 5342 Nolu sepiyolit sahasına ait maden raporu. MTA Raport No. 9727.

İrkeç, T. and Ünlü, T. (1993) An example to sepiolite

formation in volcanic belts by hydrothermal alteration: Kıbriscik (Bolu) sepiolite occurrence. *Bulletin of the Mineral Research and Exploration*, **115**, 49–68.

ITIT (1993) Utilization of sepiolitic and Mg-bearing clays in Turkey. MTA/Turkey-GIRIN/Japan Joint Research Project Final Report, ITIT Roject No. 90–1–5, 314 pp.

Jones, B.F. and Galán, E. (1988) Sepiolite and palygorskite. Pp. 631–374 in: *Hydrous Phyllosilicates (Exclusive of Micas)* (S.W. Bailey, editor). Reviews in Mineralogy, **19**, Mineralogical Society of America, Chantilly, Virginia, USA.

Kadir, S. and Eren, M. (2008) The occurrence and genesis of clay minerals associated with Quaternary caliches in the Mersin area, southern Turkey. *Clays and Clay Minerals*, **56**, 244–258.

Kadir, S. and Erkoyun, H. (2015) Characterization and distribution of fibrous tremolite and chrysotile minerals in the Eskişehir region of western Turkey. *Clay Minerals*, **50**, 441–458.

Kadir, S., Baş, H., and Karakaş, Z. (2002) Origin of sepiolite and loughlinite in a Neogene volcano-sedimentary lacustrine environment, Mihalıççık-Eskişehir, Turkey. *The Canadian Mineralogist*, **40**, 1091–1102.

Kadir, S., Eren, M., and Atabey, E. (2010) Dolocretes and associated palygorskite occurrences in siliciclastic red mudstones of the Sariyer formation (Middle Miocene), southeastern side of the Çanakkale strait, Turkey. *Clays and Clay Minerals*, **58**, 205–219.

Kaplan, M.Y., Eren, M., Kadir, S., Kapur, S., and Huggett, J. (2014) A microscopic approach to the pedogenic formation of palygorskite associated with Quaternary calcretes of the Adana area, southern Turkey. *Turkish Journal of Earth Sciences*, **23**, 559–574.

Karakaş, S.Z. (1992) Ballıhisar-İlyaspaşa (Sivrihisar-Eskişehir güneyi) yöresinin jeolojik, petrografik ve mineralojik incelenmesi. Ankara Üniversitesi Fen Bilim. Enstitüsü Doktora Tezi, Ankara, 184s (unpublished).

Karakaya, N., Karakaya, M.Ç., Temel, A., Küpeli, Ş., and Tunoğlu, C. (2004) Mineralogical and chemical characterization of sepiolite occurrences at Karapınar (Konya basin, Turkey). *Clays and Clay Minerals*, **52**, 495–509.

Karakaya, M.Ç. Karakaya, N., and Temel, A. (2011) Mineralogical and geochemical chartacteristics and genesis of the sepiolite deposits at Polatlı basin (Ankara, Turkey). *Clays and Clay Minerals*, **59**, 286–314.

Konak, N. (2002) 1/500,000 scale geological map of Turkey - İzmir, General Directorate of Mineral Research and Exploration of Turkey.

Kulaksız, S. (1981) Sivrihisar KB sının jeolojisi. *Hacettepe Üniversitesi Yerbilimleri Dergisi*, **8**, 103-124, Ankara.

Lawrence, J.R. and Taylor, H.P. Jr. (1971) Deuterium and oxygen-18 correlation: Clay minerals and hydroxides in Quaternary soil compaired to meteoric waters. *Geochimica et Cosmochimica Acta*, **35**, 993–1003.

Lawrence, J.R. and Taylor, H.P. Jr. (1972) Hydrogen and oxygen isotope systematics in weathering profiles. *Geochimica et Cosmochimica*, **36**, 1377–1393.

Moore, D.M. and Reynolds, R.C. (1989) *X-ray Diffraction and the Identification and Analysis of Clay Minerals*. Oxford University Press, New York, 332 pp.

Newman, A.C.D. and Brown, G. (1987) The chemical constitution of clays. Pp. 1–128 in: *Chemistry of Clays and Clay Minerals* (A.C.D. Newman, editor). Monograph **6**, Mineralogical Society, London.

Öncel, Z. and Denizci, F. (1982) Eskişehir bölgesi lületaşı ve magnezit etüdleri raporu. MTA raport No. 7181, Ankara, 3 V.

Özbaş, Ü. (2008) Türkiye'deki farklı sepiyolit-paligorskit oluşumlarının kökeni ve diyajenetik evrimi. Dokuz Eylül Üniversitesi Fen Bilimleri Enstitüsü Doktora Tezi, 239 s.

Post, J.L. (1978) Sepiolite deposits of the Las Vegas, Nevada area. *Clays and Clay Minerals*, **26**, 58–64.

Post, J.L. and Crawford, S. (2007) Varied forms of palygorskite and sepiolite from different geologic systems. *Applied Clay Science*, **36**, 232–244.

Pozo, M. and Casas, J.C. (1999) Origin of kerolite and associated Mg clay in palustrine–lacustrine environments. The Esquivias deposit (Neogene Madrid Basin, Spain). *Clay Minerals*, **34**, 395–418.

Rodas, M., Luque, F.J., Mas, R., and Garzon, M.G. (1994) Calcretes, palycretes and silcretes in the Paleogene detrital sediments of the Dueo and Tajo Basins,central Spain. *Clay Minerals*, **29**, 273–285.

Saraç, C., İrkeç, T., Gençoğlu, H., and Tercan, A.E. (1996) Veletler Sırtı / Kurtşeyh (Sivrihisar, Eskişehir) sepiyolit cevherleşmesinin rezerv-tenör değerlendirilmesi. *Jeoloji Mühendisliği*, **49**, 23–34.

Sarıız, K. (2000) The geology, mineralogy, and occurrence of bedded sepiolite deposits in the Akçayır-Yürükakçayır (Eskişehir) lacustrine basin, central Turkey. *Expolaration and Mining Geology*, **9**, 265–275.

Savin, S.M. and Epstein, S. (1970) The oxygen and hydrogen isotope geochemistry of clay minerals. *Geochimica et Cosmochimica Acta*, **34**, 25–42.

Şengör, A.M.C. and Yılmaz, Y. (1981) Tethyan evolution of Turkey: a plate tectonic approach. *Tectonophysics*, **75**, 181–241.

Şengör, A.M.C., Görür, N., and Şaroğlu, F. (1985) Strike-slip faulting and related basin formation in zones of tectonic escape: Turkey as a case study. Pp. 227–264 in: *Strike-Slip Deformation, Basin Formation and Sedimentation* (K.T. Biddle and N. Christie-Blick, editors). Special Publication, **37**, Society of Economic Paleontologists and Mineralogists, Tulsa, Oklahoma, USA.

Shadfan, H., Mashhady, A.S., Dixon, J.B., and Hussen, A.A. (1985) Palygorskite from Tertiary formations of eastern Saudi Arabia. *Clays and Clay Minerals*, **33**, 451–457.

Sheppard, S.M.F. (1986) Characterization and isotopic variations in natural waters. Pp. 141–162 in: *Stable Isotopes in High Temperature Geological Processes* (J.W. Valley, H.P. Taylor, and J.R. O'Neil, editors). Reviews in Mineralogy, **16**. Mineralogical Society of America, Chantilly, Virginia, USA.

Sheppard, S.M.F., Nielsen, R.L., and Taylor, H.P. (1969) Oxygen and hydrogen isotope ratios of clay minerals from porphyry copper deposits. *Economic Geology*, **64**, 755–777.

Singer, A. (1979) Palygorskite in sediments: detrital, diagenetic, or neoformed – a critical review. *Geologische Rundschau*, **68**, 996–1008.

Singer, A. (1984) Pedogenic palygorskite in the arid environment. Pp. 169–176 in: *Palygorskite-Sepiolite Occurrence, Genesis and Uses* (A. Singer and E. Galán, editors). Developments in Sedimentology, **37**, Elsevier, Amsterdam.

Singer, A. (1989) Palygorskite and sepiolite group minerals. Pp. 829–872 in: *Minerals in Soil Environments* (J.B. Dixon and S.B. Weed, editors). Soil Science Society of America, Madison, Wisconsin, USA.

Singer, A. and Norrish, K. (1974) Pedogenic palygorskite occurrences in Australia. *American Mineralogist*, **59**, 508–517.

Suárez, M. and Garcia-Romero, E. (2011) Advances in the crystal chemistry of sepiolite and palygorskite. Pp. 33–65 in: *Developments in Palygorskite-Sepiolite Research. A New Outlook on these Nanomaterials* (E. Galán and E. Singer, editors). Developments in Clay Science, Vol. **3**. Elsevier, Amsterdam.

Suárez, M. and Garcia-Romero, E. (2013) Sepiolite–palygorskite: a continuous polysomatic series. *Clays and Clay Minerals*, **61**, 461–472.

Suárez, M., Robert, M., Elsass, F., and Martin-Pozas, J.M. (1994) Evidence of a precursor in the neoformation of palygorskite – New data by analytical electron microscopy. *Clay Minerals*, **29**, 255–264.

Sun, S.S. and McDonough, W.F. (1989) Chemical and isotopic systematics of oceanic basalts: implications for mantle compositions and processes. Pp. 313–345 in: *Magmatism in the Ocean Basins* (A.D. Saunders and M.J. Norry, editors). Geological Society Special Publication, **42**. Geological Society, London.

Taylor, H.P. (1974) The application of oxygen and hydrogen isotope studies to problems of hydrothermal alteration and ore deposition. *Economic Geology*, **69**, 843–883.

Taylor, H.P. (1979) Oxygen and hydrogen relationships in hydrothermal mineral deposits. Pp. 236–277 in: *Geochemistry of Hydrothermal Ore Deposits* (H.L. Barnes, editor). 2nd edition. Wiley, New York.

Turhan, N. (2002) 1/500,000 scale geological map of Turkey – Ankara, General Directorate of Mineral Research and Exploration of Turkey.

Webster, D.M. and Jones, B.F. (1994) Paleoenvironmental implications of lacustrine clay minerals from the Double Lakes Formation, Southern High Plains, Texas. Pp. 159–168 in: *Sedimentology and Geochemistry of Modern and Ancient Saline Lakes* (R.W. Renault and W.M. Last, editors). Special Publication, **50**. SEPM–Society for Sedimentary Geology, Tulsa, Oklahoma, USA.

Whitney, D.L. and Evans, B.W. (2010) Abbreviations for names of rock-forming minerals. *American Mineralogist*, **95**, 185–187.

Wright, V.P. (1984) Peritidal carbonate facies models: A review. *Geological Journal*, **19**, 309–325.

Yeniyol, M. (1986) Vein-like sepiolite occurrence as a replacement of magnesite in Konya, Turkey. *Clays and Clay Minerals*, **34**, 353–356.

Yeniyol, M. (1992) Geology, mineralogy and genesis of the Yenidogan (Sivrihisar) sepiolite deposit. *Mineral Research and Exploration Bulletin of Turkey*, **114**, 71–84.

Yeniyol, M. (1993) Meerschaum sepiolite and palygorskite in central Anatolia. *10th International Clay Conference*, pp. 378–382, Australia.

Yeniyol, M. (2007) Characterization of a Mg-rich and low-charge saponite from the Neogene lacustrine basin of Eskişehir, Turkey. *Clay Minerals*, **42**, 541–548.

Yeniyol, M. (2012) Geology and mineralogy of a sepiolite-palygorskite occurrence from SW Eskişehir (Turkey). *Clay Minerals*, **47**, 93–104.

Yeniyol, M. (2014) Characterization of two forms of sepiolite and related Mg-rich clay minerals from Yenidoğan (Sivrihisar, Turkey). *Clay Minerals*, **49**, 91–108.

Yeniyol, M. and Öztunalı, Ö. (1985) Yunak sepiyolitinin mineralojisi ve oluşumu. *2. Ulusal Kil Sempozyumu*, s. 171–186, Ankara.

Yılmaz, Y. (1981) Sakarya kıtası güney kenarının tektonik evrimi. *Yerbilimleri*, **1**, 33–52, İstanbul.

Yüce, G., Italiano, F., Taskiran, L., Yasin, D., and Gulbay, A.H. (2015) Hydrogeochemical characteristics of low-enthalpy geothermal waters from Eskisehir Province (Turkey). Proceedings World Geothermal Congress Melbourne, Australia, 1–13.

(*Received 7 February 2016; revised 19 April 2016; Ms. 1088; AE: E. Garcia-Romero*)